Cationic homopolypeptides: A versatile tool to design multifunctional antimicrobial nanocoatings

Leyla Kocgozlu [a,b,1], Angela Mutschler [a,b,1], Lorène Tallet [a,b], Cynthia Calligaro [c], Helena Knopf-Marques [a,b], Eloïse Lebaudy [a,b], Eric Mathieu [a,b], Morgane Rabineau [a,b], Varvara Gribova [a,b], Bernard Senger [a,b], N. Engin Vrana [c,**], Philippe Lavalle [a,b,*]

[a] *Institut National de la Santé et de la Recherche Médicale, UMR_S 1121, Strasbourg, France*
[b] *Université de Strasbourg, Faculté de Chirurgie Dentaire, Strasbourg, France*
[c] *SPARTHA Medical, Strasbourg, France*

ARTICLE INFO

ABSTRACT

Postoperative infections are the most common complications faced by surgeons after implant surgery. To address this issue, an emerging and promising approach is to develop antimicrobial coatings using antibiotic substitutes. We investigated the use of polycationic homopolypeptides in a layer-by-layer coating combined with hyaluronic acid (HA) to produce an effective antimicrobial shield. The three peptide-based polycations used to make the coatings, poly(L-arginine) (PAR), poly(L-lysine), and poly(L-ornithine), provided an efficient antibacterial barrier by a contact-killing mechanism against Gram-positive, Gram-negative, and antibiotic-resistant bacteria. Moreover, this activity was higher for homopolypeptides containing 30 amino-acid residues per polycation chain, emphasizing the impact of the polycation chain length and its mobility in the coatings to deploy its contact-killing antimicrobial properties. However, the PAR-containing coating emerged as the best candidate among the three selected polycations, as it promoted cell adhesion and epithelial monolayer formation. It also stimulated nitric oxide production in endothelial cells, thereby facilitating angiogenesis and subsequent tissue regeneration. More interestingly, bacteria did not develop a resistance to PAR and (PAR/HA) also inhibited the proliferation of eukaryotic pathogens, such as yeasts. Furthermore, *in vivo* investigations on a (PAR/HA)-coated hernia mesh implanted on a rabbit model confirmed that the coating had antibacterial properties without causing chronic inflammation. These impressive synergistic activities highlight the strong potential of PAR/HA coatings as a key tool in combating bacteria, including those resistant to conventional antibiotics and associated to medical devices.

1. Introduction

Over the past decades, antibiotic resistance has become one of the major global health challenges [1–3]. The worsening of this phenomenon in recent years severely threatens our ability to control bacterial contamination, resulting in higher healthcare costs, prolonging illness duration, and leading to higher mortality rates. Implant-related interventions often cause critical infections, which reduce treatment effectiveness and may require additional surgeries [4]. In particular, *Staphylococcus aureus* (*S. aureus*) contamination is considered a primary cause of hospital-acquired infections, particularly those associated with

implant-related infections [5], or in patients with heart diseases [6,7]. In this context, it is crucial to identify new drugs and alternative treatments to combat pathogenic bacteria. Additionally, developing new strategies to prevent early post-implant infections is of utmost importance. One of the most promising strategies is a surface-based approach that locally prevents bacteria proliferation. Moreover, due to the specific regulatory and safety considerations regarding implants, approaches that do not resort to conventional drugs or modify implanted materials are desirable.

The emergence of nanotechnologies promises new perspectives and possibilities in the pathogens fight throughout the chemodynamic

therapy, photothermal therapy, starvation therapy [8] and modifications of the surface using topography, antimicrobial peptide coating, nanoparticle coating [9]. Using an antiadhesive coating, for instance by creating a water-repellent barrier with a hydrophobic coating, could inhibit pathogen adhesion and growth, which was encouraging at first [10,11]. Different combined strategy are developed to prevent pathogen adhesion and biofilm formation [12]. Nevertheless, the challenge with this approach is pathogen survival, which could colonize neighboring sites, thus maintaining a high infection risk. Another strategy involves the use of coatings containing antibiotics, representing an emerging and promising way to limit post-surgery infections. This strategy is currently implemented with long-term implanted medical devices, such as pacemakers [13,14]. However, certain disadvantages are also associated with this coating type, such as antibiotic resistance emergence, difficulty in controlling the quantity of loaded antibiotics and their release, and efficiency loss over time.

Our previous study focused on developing coatings enabling a contact-killing process, which involves a direct physical interaction between active coating polymers and the bacteria, rapidly destroying bacteria after contact with the coating. The first promising study was based on multilayer coatings built by self-assembly of poly(L-arginine) and hyaluronic acid (PAR/HA) on surfaces, using the layer-by-layer (LbL) method. These LbL films made with polyaminoacids and polysaccharides depict most of the time an exponentially growing regime mainly due to diffusion of polymer chains in and out the whole film section [15]. These coatings have demonstrated interesting immunomodulatory properties, coupled with antimicrobial properties against *S. aureus* [16]. Moreover, another study has provided a deeper understanding on the antimicrobial activities of PAR, highlighting the importance of PAR chain length [17]. More precisely, multilayer films (PAR/HA) containing PAR with 30 arginine residues (PAR30) presented a strong antimicrobial activity against a wide range of pathogens, both Gram-positive and Gram-negative, including *S. aureus*, methicillin-resistant *S. aureus* (MRSA), *Micrococcus luteus* (*M. luteus*), *Escherichia coli* (*E. coli*), and *Pseudomonas aeruginosa* (*P. aeruginosa*). Moreover, the contact-killing antimicrobial effect was only possible in a narrow range of combinations by precisely controlling the self-assembly of PAR with the polyanion. For films composed of PAR chains containing residue numbers lower or higher than 30 (PAR10, PAR100, or PAR200), no antibacterial activity was monitored. The absence of antimicrobial properties in the (PAR100/HA) or (PAR200/HA) films could be attributed to the significantly lower PAR chain mobility within these films, limiting diffusion beyond the film. In contrast, PAR chains in PAR30/HA films showed nearly 90 % of mobility, leading to an antibacterial activity. We also demonstrated that the (PAR/HA) film thickness increased with the number of arginine residues contained in the PAR chains. As a consequence, (PAR10/HA) being the thinnest of the films tested, the amount of PAR10 was not sufficient to induce antimicrobial activity due to a lack of adequate PAR10 amounts to induce antimicrobial activity. Finally, (PAR30/HA) films met the physicochemical conditions mentioned to deploy a strong antimicrobial property through a contact-killing process.

The next study compared different polyanions interacting with PAR30 polycations during multilayer film construction [18]. This approach highlighted the role of polyanions in the final antimicrobial properties of multilayer films composed of (PAR30/polyanions). Different polyanion types were tested in combination with HA. The first group was represented by the same family as the HA molecule, *i.e.,* anionic polysaccharides such as alginate (ALG), heparin (HEP), and chondroitin sulfate A (CSA). In addition to polyanions, a homopolypeptide, poly(L-glutamic acid) (PGA) and a synthetic polyelectrolyte, poly(sodium 4-styrene sulfonate) (PSS), were also used. Unsurprisingly, only PAR as a polycation possessed strong antimicrobial activity by itself, as polyanions were not active against *S. aureus*. Secondly, HA surprisingly remained the only polyanion providing an antimicrobial activity in the coating when associated with PAR30.

(PAR30/ALG), (PAR30/HEP), (PAR30/CSA), (PAR30/PGA), or (PAR30/PSS), with the same number of (polycation/polyanion) bilayers, formed multilayer films with approximately the same thickness but did not show any antibacterial activity [18]. The major role of HA in this context was related to its ability to only establish weak interactions with PAR30, thus facilitating the PAR30 chain diffusion within the (PAR30/HA) multilayer films compared with the other PAR30/polyanion coatings [18]. PAR30 interaction with the other polyanions was probably too strong, preventing PAR30 diffusion in the film, and thus any activity against bacteria.

After establishing the polyanion contribution, the next challenge was to determine whether the coatings' antimicrobial activity could be achieved using other cationic homopolypeptides associated with HA. Moreover, we sought to establish whether there was a similarity among these homopolypeptides in terms of effectiveness of a specific chain length, similar to what was observed with polyarginine. Lysine and ornithine, two other natural cationic amino acids with intrinsic antimicrobial properties and an ability to be assembled as LbL films, were potentially of major interest. Hence, in the present study, we investigated films based on i) poly(L-lysine) (PLL) and poly(L-ornithine) (PLO) as polycations with various residue numbers (30, 100, and 250) and ii) on HA as polyanion. We compared them with PAR-based films (Table 1). By varying the residue number of all polycations, we determined if the selection of 30 residues for optimal activity, as demonstrated for PAR, was a "golden number".

Although the antimicrobial effect of PLL and PLO polymers in their free state has been previously established [19–22], their antimicrobial activity when incorporated into an LbL film, particularly in combination with HA, has not yet been thoroughly evaluated. Thus, a deep analysis in terms of physicochemical properties, biocompatibility, and biological activities of these homopolypeptide/HA coatings was performed. Furthermore, their efficiency was evaluated *in vivo* using an animal model. Recent studies have highlighted a clinical issue with visceral/parietal implants in hernia repair [23,24]. Relatively low infection rates have been reported (between 1 % and 4 %) [25]. However, 20 million hernia repair meshes are implanted worldwide and it is estimated that about 60 000 repairs are infected annually in the USA, highlighting the urgent need to address this issue [26]. One potential solution to prevent these hernia mesh infections is the local administration of anti-infective agents. Our LbL coatings could offer such suitable approach.

This new study was divided into three parts. First, results highlighted the antimicrobial activity of the newly-developed coatings and opened new perspectives in the strategies against resistant pathogens and ESKAPEE pathogens (*Enterococcus faecium, Staphylococcus aureus, Klebsiella pneumoniae, Acinetobacter baumannii, Pseudomonas aeruginosa, Enterobacter* spp., and *E. coli*) [27,28]. Second, we explored their interactions with eukaryotic cells by assessing biocompatibility, cell adhesion to the coating, epithelium formation, and NO (nitric oxide) production by endothelial cells cultured on the coating. Finally, an *in vivo* study was performed on a rabbit model of parietal mesh infections to evaluate bacteria adhesion on the meshes, assess tissue state, and monitor the inflammatory response. This last part complemented the *in vitro* results and helped us select the best homopolypeptide/HA candidate for the coating of implants involved in hospital-related infections.
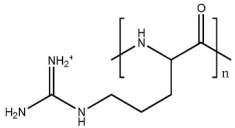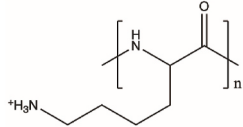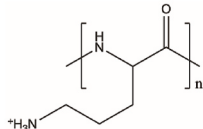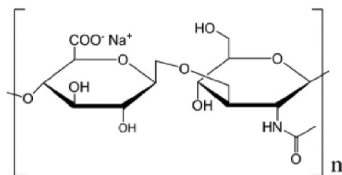
2. Materials and methods

2.1. Polyelectrolytes

The following polyelectrolytes were used to build the multilayer films. Polycations: poly(L-arginine hydrochloride), poly(L-lysine hydrochloride), and poly(L-ornithine hydrobromide) were purchased from Alamanda Polymers, USA. Different PAR polymers were studied according to the number of arginines (R) per chain: PAR30 (30R, Mw [molecular weight] = 6.4 kDa), PAR100 (100R, Mw = 20.6 kDa), and

Table 1

Chemical structures of the polycations poly(ʟ-arginine) (PAR), poly(ʟ-lysine) (PLL), poly(ʟ-ornithine) (PLO) and the associated polyanion hyaluronic acid (HA).

Name of products	Chemical structure	Notation	Molecular weight (Da)
Poly(ʟ-arginine)		PAR10	2100
		PAR30	6400
		PAR100	20 600
		PAR200	40 800
Poly(ʟ-lysine)		PLL10	1600
		PLL30	5400
		PLL100	17 300
		PLL250	39 500
Poly(ʟ-ornithine)		PLO30	5900
		PLO100	18 500
		PLO250	50 300
Hyaluronic acid		HA	150 000

PAR200 (200R, Mw = 40.8 kDa). Different PLL polymers were studied according to the number of lysines (K) per chain: PLL10 (10K, Mw = 1.6 kDa), PLL30 (30K, Mw = 5.4 kDa), PLL100 (100K, Mw = 17.3 kDa), and PLL250 (250K, Mw = 39.5 kDa). Different PLO polymers were studied according to the number of ornithines per chain: PLO30 (30 ornithine residues, Mw = 5.9 kDa), PLO100 (100 ornithine residues, Mw = 18.5 kDa), and PLO 250 (250 ornithine residues, Mw = 50.3 kDa). The polyanion was HA (Mw = 150 kDa) and purchased from Lifecore Biomed, USA.

2.2. Construction of (polycations/HA)$_n$ films

For multilayer construction, 24 and 48 bilayers of (polycations/HA) were built by using an automated dipping robot (Riegler & Kirstein GmbH, Berlin, Germany). Glass slides were previously washed with Hellmanex® II solution at 2 %, H$_2$O, pure ethanol, and dried with compressed air. PAR30, PLL30, PLO30, and HA were dissolved in a sterilized buffer containing 150 mM NaCl and 10 mM of tris (hydroxymethyl)-aminomethane (TRIS, Merck) at pH 7.4 ("NaCl-Tris buffer"). The concentration for each polyelectrolyte was 0.5 mg.mL^{-1}. Glass slides were consecutively dipped in polycation, rinsing solution, and polyanion baths. After construction, films were dried, immersed in NaCl-Tris buffer and stored at 4 °C before use.

2.3. Film construction characterization (quartz crystal microbalance)

Film production was followed *in situ* using a quartz crystal microbalance with dissipation monitoring (QCM-D, E1, Q-Sense, Sweden). Quartz crystals coated with a titanium dioxide (TiO$_2$) or a polypropylene layer (Q-Sense) were excited at their fundamental frequency (about 5 MHz), as well as at the third, fifth, and seventh overtones (noted $\nu = 3, 5$, and 7, corresponding respectively to 15, 25, and 35 MHz). Changes in the resonance frequencies (Δf_ν) and dissipation values (ΔD) were measured at these three frequencies. As an approximation, an increase of the normalized frequency variation ($-\Delta f_\nu/\nu$) is associated to a proportional mass increase coupled with the quartz (Sauerbrey's approximation). However, when normalized frequency shifts for the various overtones are unequal, it is recommended to apply the model proposed by Voinova et al., in which both measured frequency shifts and dissipations for several overtones are used to derive the thickness [29]. This model is based on the hypothesis that the film deposited on the quartz crystal is homogeneous, isotropic, and a non-sliding viscoelastic stratum. Nanofilm thicknesses presented in this study were estimated using data corresponding to the overtones $\nu = 3, 5$, and 7.

For *in situ* film construction, a peristaltic pump was used at a flow rate of 250 µL min^{-1} to inject 400 µL of each solution in the QCM-D fluid liquid cell (cell volume was about 40 µL). The bottom of the cell was formed by the quartz crystal sensor itself. During the whole experiment, the QCM sensor was maintained at 25 °C. PAR30, PLL30, PLO30, and HA were dissolved at 0.5 mg.mL^{-1} in NaCl-Tris buffer. These polyelectrolytes were successively injected into the cell containing the quartz crystal, starting with the polycation solution. They were left to adsorb for 8min and after each deposition, a rinsing step of 5min with NaCl-Tris buffer was performed.

2.4. Fluorescent labeling of polycations

For polycation chain labeling, PAR, PLL, and PLO (dissolved at 1 mg. mL^{-1} in 100 mM NaHCO$_3$ buffer, pH 8.3) were incubated with fluorescein isothiocyanate (FITC, Sigma-Aldrich, France) at a 1:2 M ratio of polycations/FITC at room temperature for 3 h. This solution was dialyzed with a Slide-A-Lyzer Dialysis Cassette (ThermoFischer Scientific Inc., USA) with a cut-off of 3500 molecular weight cut-off (MWCO), against 1 L of water at 4 °C for 24 h, then 1 L of NaCl-Tris buffer for 24 h. The resulting polycation-FITC was stored at 0.5 mg.mL^{-1} in NaCl-Tris buffer at −20 °C. Following the same process, PAR30 (dissolved at 1 mg.mL^{-1} in 100 mM NaHCO$_3$ buffer, pH 8.3) was incubated with tetramethylrhodamine (TRITC, Sigma-Aldrich, France) at a 1:2 M ratio of polycation/TRITC at room temperature for 3 h. This solution was dialyzed with a Slide-A-Lyzer Dialysis Cassette (ThermoFischer Scientific Inc., USA), with a cut-off of 3500 MWCO, against 1 L of water at 4 °C for 24 h, then 1 L of NaCl-Tris buffer for 24 h. PAR30-TRITC was then produced and stored in 2 mL aliquots (0.5 mg.mL^{-1} in NaCl-Tris buffer).

2.5. Film characterization

Multilayer thickness was measured by deposition of 100 μL of polypeptide (PAR, PLL or PLO), conjugated with FITC at 0.5 mg.mL^{-1} in NaCl-Tris buffer on the multilayer films for 5min. After diffusion of polypeptide-FITC, films were washed and observed with a Zeiss LSM 710 confocal laser scanning microscope (Heidelberg, Germany) using a 20 × objective (Zeiss, Plan Apochromat).

2.6. Antibacterial assay of (polycation/HA)$_n$ films

A *S. aureus* (ATCC 25923) strain was used to assess the antibacterial properties of the test samples. The bacterial strain was cultured aerobically at 37 °C in a Mueller Hinton Broth (MHB) medium (Merck, Germany) at pH 7.4. A colony was transferred to 10 mL of MHB medium and incubated at 37 °C for 20 h, to provide a final density of 10^6 colony forming unit (CFU).mL^{-1}. To obtain bacteria in the mid-logarithmic growth phase, the absorbance (or optical density [OD]) of overnight culture at 620 nm was adjusted to 0.001.

Glass slides coated with (polycation/HA)$_{24}$ films were sterilized by using ultraviolet light for 15min, then washed with NaCl-Tris buffer. After washing, each glass slide was deposited in a 24-well plate with 300 μL of *S. aureus*, OD$_{620}$ = 0.001, and incubated for 24 h at 37 °C under agitation.

For negative control, uncoated glass slides were incubated with *S. aureus* solution. For positive control, tetracycline (10 μg.mL^{-1}) and cefotaxime (0.1 μg.mL^{-1}) were added to the *S. aureus* solution in contact with uncoated glass slides. After 24 h, the supernatant was removed and OD at 620 nm was measured. MRSA, *M. luteus* (ATCC 9341), *E. coli* (ATCC 25922), and *P. aeruginosa* (ATCC 27853) were also tested with (polycation/HA)$_{24}$ and cultured in MHB in the same conditions as previously described [17].

To evaluate the health of bacteria present on the surface, the BacLight™ RedoxSensor™ CTC Vitality Kit (Thermo Fischer Scientific Inc., USA) was used. This kit provides effective reagents for evaluating bacterial health and vitality. The kit contains 5-cyano-2,3-ditolyl tetrazolium chloride (CTC), allowing us to evaluate the respiratory activity of *S. aureus*. Indeed, healthy cells will absorb and reduce CTC into an insoluble, red, and fluorescent formazan product. Cells not respiring or respiring at slower rates than healthy cells will reduce less CTC, and consequently produce less fluorescent product, giving a semiquantitative estimate of healthy vs. unhealthy bacteria. SYTO® 24 green-fluorescent nucleic acid stain is used for counterstaining all bacteria. For the test, a solution of 50 mM CTC and 0.001 mM Syto 24 in distilled water was prepared. Each glass slide was washed with phosphate-buffered saline (PBS) at pH 7.4. Then, 270 μL of PBS and 30 μL of CTC/SYTO 24 solution were added per slide. The plates were incubated for 30min at 37 °C, away from light. Each surface was then studied using confocal microscopy (Zeiss LSM 710 microscope, Heidelberg, Germany) with a 63 × objective, immersed in oil. Excitation/emission wavelengths of the dyes were 450/630 nm for CTC and 490/515 nm for SYTO 24.

2.7. Fluorescent recovery after photobleaching

To determine the difference between the mobility of the homopolycations, the diffusion coefficient (*D*) and the proportion of mobile molecules (*p*) were measured for PAR30, PLL30, and PLO30 coupled with FITC in (polycation30-FITC/HA)$_{24}$ multilayers by photobleaching experiments (FRAP, fluorescence recovery after photobleaching).

A slide coated with the multilayer was introduced in a home-made sample holder and immersed in 200 μL of NaCl-Tris buffer, to prevent the multilayer from drying during the experiments. Two circular regions R4 (4.4 μm in radius in a 35μm × 35 μm image) and R10 (10.6 μm in radius in a 85μm × 85 μm image) were exposed to an intense laser pulse at the absorbing wavelength of the FITC (λ = 488 nm). Then,

fluorescence recovery in the bleached area, which is due to the mobility of the labeled molecules in the non-bleached area, was monitored over time. Observations were made using a Zeiss LSM 710 microscope (Heidelberg, Germany) with a 20 × objective (Zeiss, Plan Apochromat). Three samples per condition were analyzed.

2.8. Cell culture

The Balb/3T3 (ATCC CCL163) mouse embryonic fibroblast cell line was cultured at 37 °C in DMEM (Dulbecco's Modified Eagle Medium, Invitrogen) with 10 % of FBS (fetal bovine serum, Invitrogen), 100 μg. mL^{-1} penicillin, and 100 μg.mL^{-1} streptomycin (Invitrogen). Madin-Darby canine kidney (MDCK) strain II was cultured in low-glucose DMEM supplemented with 100 μg.mL^{-1} penicillin, 100 μg.mL^{-1} streptomycin (Invitrogen), and 10 % FBS (Invitrogen). HUVECs (human umbilical vein endothelial cells) were cultured in human endothelial medium (Invitrogen) completed with 100 μg.mL^{-1} penicillin, 100 μg. mL^{-1} streptomycin (Invitrogen), and 10 % FBS (Invitrogen).

2.9. Cytotoxicity assays

Cytotoxicity assays were conducted following the ISO 10993-5 guidelines (Biological Evaluation of Medical Devices, Part 5: Tests for *in vitro* cytotoxicity using Balb/3T3 cells).

A coating built on glass slides was incubated in complete cell culture medium at 37 °C for 72 h. Then, the supernatant ("extract 100 %") was diluted in complete cell culture medium to obtain concentrations of 50 %, 25 % and 12.5 % (volume per volume [v/v]).

Balb/3T3 cells were seeded in 96-well plates, treated with the 100 % extracts and diluted extracts, and incubated at 37 °C with 5 % CO$_2$ for 24 h. Following incubation, treatment was removed, 3-(4,5-dimethylthiazol-2-yl)-2,5-diphenyltetrazolium bromide (MTT) solution was distributed in each well, and incubated at 37 °C with 5 % CO$_2$ for 2 h. The MTT solution was then removed, dimethyl sulfoxide was added, and the resulting solution was quantified by absorbance measurement at 556 nm. The cytotoxicity for different concentration of arginine and chlorhexidine solutions (Sigma-Aldrich) was evaluated in the same culture conditions.

2.10. Cell adhesion characterization by atomic force microscopy

Samples for atomic force microscopy (AFM) were prepared with MDCK cells seeded on glass substrate, (PAR30/HA)$_{24}$, (PLL30/HA)$_{24}$, and (PLO30/HA)$_{24}$ films. After 24 h of culture, cells were fixed with paraformaldehyde (PFA) 4 % in PBS, and samples were dehydrated in ethanol solutions increasing successively from 50 % to 70 %, 90 %, and 100 %.

AFM images were obtained using "contact" mode in air with the Multimode Nanoscope VI from Bruker (Santa Barbara, CA). Cantilevers with a spring constant of 0.03N.m^{-1} and silicon nitride tips were used (model ScanAsyst-Air-HR, Bruker). Several scans over a given surface area were performed. The scans led to reproducible images to confirm that no sample damage was induced by the tip and that observations were valid over large surface areas. Image size was 150μm × 150 μm.

2.11. Cell adhesion characterization by scanning electron microscopy

Samples for observation with scanning electron microscopy (SEM) were prepared with MDCK cells seeded on glass substrate or (PAR30/HA)$_{24}$ films. After 24 h of culture, cells were fixed with a solution composed of 4 % PFA and 1 % glutaraldehyde in 200 mM 4-(2-hydroxyethyl)-1-piperazineethanesulfonic acid (HEPES) buffer at pH 7.4. Then, samples were dehydrated in ethanol solutions increasing successively from 50 % to 70 %, 90 %, and 100 %. After another desiccation step at critical point and metallization, samples were ready for the observation using Quanta 250 FEG SEM (FEI Company,

Eindhoven, Netherlands).

2.12. Immunofluorescence microscopy

Cells were seeded at a density of 2×10^5 cells.cm^{-2} on all the studied substrates and cultured for 24 h. Cells were then fixed and permeabilized for 15 min in 3.7 % (w/v) PFA and 0.1 % (v/v) Triton X-100 in PBS. After fixation, cells were incubated for 1 h in 10 % (v/v) FBS in PBS. Actin and DNA staining were realized by incubating the cells with Alexa Fluor 568 phalloidin (1 μg/mL, Invitrogen, A12380) and Hoechst 33258 (5 μg. mL^{-1}) respectively. For this study, the following mouse anti-human antibodies were used with a dilution of 1:100: anti-vinculin (clone hVin-1, Sigma-Aldrich, V9131), in combination with the corresponding Alexa Fluor 488-conjugated secondary goat anti-mouse antibody (1:500; Invitrogen, A-11001). Fluorescence images were acquired using a Zeiss LSM710 confocal microscope (Heidelberg, Germany).

2.13. NO generation

To assess the effect of PAR on NO secretion by endothelial cells, as NO secretion is crucial for capillary ingrowth induction towards the implant sites, NO levels were quantified via nitrite detection in the supernatant in cell experiments with HUVECs. The nitrate/nitrite fluorometric assay kit from Cayman chemical (USA) was used, and the test was performed according to manufacturer's instruction. This experiment was performed with HUVECs seeded on the film surfaces (*direct*) and with HUVECs seeded on the standard plastic tissue culture inserts put in contact with the medium where films were immersed (*indirect*). Supernatants were analyzed after 1, 3, and 7 days of culture.

2.14. Resistance acquisition assay

To test whether bacteria can develop resistance against homopolycations, the minimal inhibitory concentrations (MICs) of *S. aureus* to PAR30 and tetracycline were determined by microdilution in MHB according to Clinical and Laboratory Standards Institute guidelines. *S. aureus,* at 10^6 CFU.mL^{-1}, were seeded at twofold serial dilutions in 96-well plates in the presence of PAR30 or tetracycline. *S. aureus* growth was evaluated after incubation at 37 °C after 24 h by measuring OD at 620 nm. MIC was defined as the lowest concentration of PAR30 or tetracycline preventing visible growth.

S. aureus were grown in MHB in continuous presence of PAR30 or tetracycline concentration corresponding to half of the MIC. MIC was evaluated every 3–4 days, then concentrations of PAR30 and tetracycline in *S. aureus* culture were adjusted to conform to the new half MIC assessment. Daily passages of *S. aureus* at 10^6 CFU.mL^{-1} were performed for 30 days.

2.15. Antibacterial assay of (PAR30/HA)$_{24}$ and (PAR30/HA)$_{48}$ films following the antibacterial ISO 22196 method

E. coli (ATCC 8739), *P. aeuroginosa* (ATCC 9027), *Staphylococcus epidermidis* (*S. epidermidis*, ATCC 35983), *S. aureus* (ATCC 6538), MRSA, *Enterococcus faecalis* (*E. faecalis,* ATCC 29212), and *Candida albicans* (*C. albicans,* ATCC 10231) were tested following the antibacterial ISO 22196 method for (PAR30/HA)$_{24}$ and (PAR30/HA)$_{48}$ films. Two subcultures were grown at 35 °C during 16 h on nutrient medium for each strain, and microorganism suspensions were prepared and adjusted to 10^6 CFU.mL^{-1} in MHB. These suspensions served as inocula for *in vitro* antibacterial activity assay on the tested surfaces at 35 °C. After 24 h of incubation of the corresponding pathogens, antibacterial activity was neutralized by adding Letheen broth and inoculated on tryptone soy agar yeast (TSYEA) plates (Sigma Aldrich). After incubation at 35 °C for 24 h, colonies grown on plates were counted and microorganism counts were calculated as log CFU/sample.

2.16. Super resolution microscopy assay

E. coli (ATCC 2146), resistant to ampicillin and kanamycin, and producing the green fluorescent protein (GFP), were cultured on glass dishes (IBIDI) at 37 °C in MHB. PAR30-TRITC at 0.02 mg.mL^{-1} was added to the medium for 30 min and rinsed with PBS, then fixed with 4 % PFA. The sample was imaged with the Nikon A1 N-SIM using a high-magnification objective (100 ×).

2.17. In vivo assay

A clinically relevant approach for assessing antimicrobial mesh prototypes was developed using a preclinical rabbit model described by Fernández-Gutiérrez et al. in 2013 [30]. This model has also been successfully used for the comparative evaluation of other antimicrobial mesh materials such as DualMesh Plus or polypropylene meshes soaked in different antiseptic solutions [31,32]. The *in vivo* assay in the present study was performed in collaboration with the University of Alcalá (Madrid, Spain).

2.17.1. Experimental animals and ethics

The experimental animals used were specific pathogen-free male New Zealand white rabbits weighing approximately 3,000 g. A total of 21 animals were utilized. The study was carried out in strict accordance with the Guide for the Care and Use of Laboratory Animals of the National and European Institutes of Health (Spanish Law 6/2013, Spanish Royal Decree 53/2013, European Directive 2010/63/UE and European Convention of the Council of Europe ETS123). All procedures were performed at the University of Alcalá's animal research center. The protocol was approved by the local Ethics Committee on Animal Experiments (reference PROEX160/16).

2.17.2. Mesh implants and study groups

The hernia repair material used was Optilene Mesh Elastic (B. Braun, Melsungen, Germany), which is a lightweight (48 g m^{-2}), reticular, and monofilament polypropylene mesh (Fig. S1a), with a pore size of 7.64 ± 0.32 mm^2. This material was cut into of 5 × 2cm fragments, which were divided into the following study groups (n = 7 each):

- Group #1: Meshes without any coating (control group)
- Group #2: Meshes coated with (PAR30/HA)$_{24}$ consisting in 24 bilayers of PAR/HA layers
- Group #3: Meshes soaked in aqueous 0.05 % chlorhexidine (CHX). This is a conventional protocol often used by surgeons.

Given that the number of animals included in the study was high (n = 21), the surgical procedure was carried out in four steps, to ensure adequate animal housing and proper handling. Meshes included in each step were randomly selected. These surgeries were scheduled in accordance with the animal research center housing availability, so that the time lapse from one surgical intervention to another was minimized.

2.17.3. Analgesia and anesthesia

Prior to surgery, analgesics were administered to the animals:

- Meloxicam (Meloxidyl®, 0.23 mg kg^{-1}) the day before the surgery (*per os*)
- Meloxicam (0.06 mg kg^{-1}) 30–60min before the surgery (subcutaneous [sc])
- Buprenorphine (Buprecare®, 0.012 mg kg^{-1}) 30–60min before the surgery (sc)

Fifteen minutes before the surgery, animals were anesthetized (intramuscular [im]) using a mixture of ketamine hydrochloride (Ketolar®, 70 mg kg), diazepam (Valium, Roche, Spain, 1.5 mg kg^{-1}), and chlorpromazine (Largatil®, 1.5 mg kg^{-1}).

2.17.4. Bacterial inocula

The *S. aureus* bacterial strain ATCC25923 from the Spanish Type Culture Collection (CECT, Valencia, Spain) was used, with a target load of 10^6 CFU.mL^{-1}.

To prepare the inoculum, bacteria were plated on lysogeny broth (LB) agar plates and incubated for 24 h at 37 °C. Then, a single colony was inoculated into 25 mL of LB broth and incubated overnight at 37 °C. Absorbance (OD$_{600}$) was read and adjusted with sterile 0.9 % saline to an OD$_{600}$ equivalent of approximately 5×10^8 CFU.mL^{-1}. This was considered as the "mother suspension". To obtain the target bacterial load of 10^6 CFU.mL^{-1}, two tenfold serial dilutions were prepared in sterile saline solution. These inocula were prepared immediately before surgery and stored in cool conditions during the whole proceeding (iced box, ~4 °C).

The number of viable CFU in the inoculation suspensions were determined by the spot plaque method in triplicate. Using the 10^6 CFU. mL^{-1} inoculum, five tenfold serial dilutions were prepared and 100 μL of each dilution plated on LB agar plates. After 24 h of incubation at 37 °C, CFU.mL^{-1} were determined for each plate and viable CFUs were calculated using the following equation:

CFU.mL^{-1} = number of CFU x dilution factor (10x)/volume plated (0.1 mL).

2.17.5. Surgical technique

Using a sterile technique, a partial thickness defect (5 × 2cm) was created on the lateral right side of the abdominal wall, removing the external and internal oblique muscles, keeping the transverse muscles, transversal fascia, and parietal peritoneum to avoid contact between microorganisms and the visceral peritoneum (Fig. S1b). In all specimens, the surgical defect was inoculated with 0.25 mL of the bacterial suspension (containing approximatively 1 to 1.5×10^6 CFU) and immediately fixed with the corresponding mesh concept, which was secured to the edges of the defect using a 4/0 polypropylene suture. Skin tissue was closed by simple interrupted stitches with a 3/0 silk suture (Fig. S1b).

During the study period and before euthanasia, rabbits were visually monitored for signs of surgical incision dehiscence, seroma formation, surgical site infection, or any other complications. Animals were weighed weekly. Before visual monitoring, staff was trained to observe behavioral and morphological characteristics associated with distress, which may specifically include for rabbits: weight loss, reluctance to move, reduced appetite/fluid intake, depression, tachypnea, and tachycardia.

Meloxicam (0.1 mg/kg) was administered *per os* mixed with water for 4 postoperative days. If pain symptoms persisted for several hours, buprenorphine (0.015 mg/kg) was also administered sc. If symptoms had persisted for more than 48 h, animals would have been euthanized. Animals with evident clinical signs of septicemia would also have been euthanized.

At 14 days after surgery, animals were sedated with up to 20 mg/kg xylazine (im) and then euthanized in a CO_2 chamber following approved protocols for experimental animal euthanasia.

2.17.6. Macroscopic observations

During necropsy, tissue reaction at implantation site in all groups was visually inspected to collect the most relevant infection-related findings, such as skin necrosis/fistula, edema or seroma formation, presence and distribution of purulent material, and degree of vascularization and tissue integration. To evaluate these findings, a scoring table previously designed for other studies was used [31].

2.17.7. Sample collection

Tissue explants were collected after skin flap creation over the intramuscular surgical site. They included the mesh itself with underlying and overlying attached tissues and surrounding tissues. They were cut into different tissue blocks, in the same way for all explants according to a patron, for morphological analysis, immunolabeling

protocols, and bacterial count on meshes, according to a precise diagram (Fig. S1c).

Blood aspirates were collected in heparinized tubes at two different time-points: surgical intervention (day 0) and euthanasia (day 14). Blood was centrifuged (10min, 1,500 g, 4 °C) to obtain plasma samples, which were aliquoted in 1.5 mL Eppendorf tubes and stored at −80 °C until cytokine assays.

2.17.8. Quantification of bacterial adhesion to the implant

Tissue blocks dedicated to bacterial adhesion analysis represented about 2/5 of the original mesh surface (two blocks: "lateral" and "central"). Samples were immersed in sterile glass tubes containing 20 mL of neutralizing pharmacopoeia diluent (NPD, 8.5 g NaCl, 2.5 mL Tween-80, 0.35 g soya lecithin, 997.5 mL distilled water). Under sterile conditions, bacteria extraction was facilitated by removal of surrounding tissues from the mesh explant and by scraping both sides of the mesh explant with a scalpel blade. The whole was subjected to a 10min sonication pulse at 40 kHz using a Bransonic 2510-DHT ultrasonic cleaning bath (Branson Ultrasonics, CT, USA). After sonication, glass tubes containing the NPD, mesh, removed tissues, and scalpel blade were thoroughly vortexed for 1min. Scalpel blades and surrounding tissues were carefully discarded, and the supernatant was used to perform five 1/10 serial dilutions. A volume of 100 μL of each dilution was seeded onto LB plates. Plates were counted at 24 h post-seeding. Viable CFU numbers were calculated, and results were expressed as viable CFU numbers per mesh explant.

2.17.9. Morphological studies

Fragments of the different implants were analyzed by light microscopy (LM) and SEM.

For LM, tissue blocks were fixed in F13 solution, embedded in paraffin, cut into 5 μm sections, and stained with hematoxylin eosin and Masson's trichrome (Goldner-Gabe). These specimens were examined under a Zeiss light microscope (Carl Zeiss, Oberkochen, Germany).

For SEM, tissue blocks were fixed in glutaraldehyde 3 %, placed in Millonig buffer (pH 7.3) and dehydrated in a graded ethanol series. Critical point was reached in an E−3000 Polaron instrument (Polaron Ltd., England) for tissue desiccation and subsequent samples were metalized with gold palladium. These specimens were examined under a Zeiss scanning electron microscope (DSM-950).

2.17.10. Immunohistochemical study

The immunohistochemical technique involved a specific monoclonal antibody to label any remaining bacteria in the implant. Paraffin-embedded tissue slides were deparaffinized, hydrated, and subsequently equilibrated in tris-buffered saline (TBS, pH 7.4). Non-specific protein interactions were blocked with 3 % bovine serum albumin (BSA). Sections were incubated with a specific mouse monoclonal anti *S. aureus* antibody (ab37644, Abcam, Cambridge, UK) in the alkaline phosphatase-labeled avidin-biotin procedure. The method included the following steps: incubation with the primary antibody (1:500 in TBS) for 60min, incubation with immunoglobulin G and biotin (1:1000 in TBS) for 45min, and labeling with streptavidin alkaline phosphatase (1:200 in TBS) for 60min. These steps were conducted at room temperature. Negative controls were subjected to 3 % BSA instead of the primary antibody. Images were revealed using a chromogenic substrate containing naphthol phosphate and fast red. Cell nuclei were counterstained for 1min with acid hematoxylin. Immunostaining was qualitatively evaluated.

2.17.11. Cytokine detection at plasmatic levels

Fresh plasma was aliquoted and stored frozen (−80 °C) until sample collection completion. At least 1.5 mL of plasma was required for each sample, ensuring enough volume to develop the enzyme-linked immunosorbent assay (ELISA) plasmatic levels of several cytokines at days 0 and 14. Interferon-γ (IFN-γ), interleukin-6 (IL-6), interleukin-10 (IL-

10), and tumor necrosis factor-α (TNF-α) were quantified via ELISA, using rabbit-specific kits, and following the manufacturer's instructions (Cusabio Technology LLC, Houston, TX, USA). For every kit used, absorbance was read at 450 nm using an iMark microplate reader (Bio-Rad Laboratories Inc, Hercules, CA, USA).

2.17.12. Statistical analysis

All macroscopic and morphological studies were qualitatively evaluated. Quantification of bacterial yields collected via sonication was expressed as mean, median, maximum, and minimum values. Data were compared among the implant groups using the Mann-Whitney *U* test. All statistical analyses were performed using the GraphPad Prism 5 software for Windows. Level of significance was set at $p < 0.05$.

3. Results and discussion

3.1. Physicochemical properties of homopolypeptide/HA films

As a first step, we targeted two new cationic homopolypeptides, PLL and PLO, and evaluated their assembly with HA into (polycations/HA) films. They were compared to the previously studied antimicrobial PAR/ HA films. The first objective was to analyze the physicochemical properties of the (PLL/HA) and (PLO/HA) films, and in particular to monitor their construction regime during the LbL deposition. We first characterized the growth of the (polycation30/HA) multilayer films using QCM-D. The normalized frequency variation ($-\Delta f_\nu/\nu$) was reported as a function of the number of deposition steps of the polycation and HA. Growth evolution of the corresponding films studied for seven bilayers exhibited an exponential regime with a similar growth regime for (PAR30/HA) and (PLL30/HA), whereas the (PLO30/HA) film showed a growth rate 50 % lower (Fig. 1a). From raw dissipation QCM data (data not shown), it appears that normalized dissipations values ($-\Delta D_\nu/\nu$) are higher in the case of PLL30/HA (between 100.10^{-6} to 130.10^{-6}) compared to PAR30/HA (between 30.10^{-6} to 70.10^{-6}) or PLO30/HA (between 40.10^{-6} to 50.10^{-6}). This indicates that PLL30/HA film is the softer and the most hydrated one which can explain its highest thickness.

The exponential growth regime observed in this study is typically related to diffusion processes of the chains in the film, as demonstrated in previous studies [33–36]. Estimation of the corresponding thicknesses using the Voinova model, as previously described, depicted that the PLL30/HA film was thicker than the two others. When comparing film thickness with the same number of deposited layers (*i.e.*, (polycation/HA)₇ films), (PLO30/HA) was about 88 nm thick, (PAR30/HA) was about 104 nm thick, and (PLL/HA) had a thickness greater than 193 nm (Fig. 1b).

Thicknesses were also roughly estimated with confocal microscopy after 24 deposited bilayers (*i.e.,* (polycation30/HA)₂₄) using fluorescently-labeled polycations (with FITC). All thicknesses were about 1 μm for (PAR30^{FITC}/HA)₂₄ and (PLO30^{FITC}/HA)₂₄ films, and 2 μm for (PLL30^{FITC}/HA) (Fig. S2). However, it is important to note that the confocal microscope z-resolution was about 500 nm. More interestingly, these images showed a uniform distribution of the fluorescent dye over the surface for all films, indicating homogenous film formation at the micrometer scale.

3.2. Homopolypeptide antimicrobial and antifungal properties

We investigated the antimicrobial activity of the selected polycations in solution as a function of their chain length and concentration to determine the MICs against *S. aureus,* a Gram-positive bacterium. MIC is defined as the lowest concentration of antimicrobial compounds inhibiting the visible growth of a microorganism after 24 h of incubation, indicating a bacteriostatic effect. As underlined in a previous study [17], for concentrations greater than 0.025 mg.mL^{-1}, all tested PARs displayed strong antimicrobial activities against *S. aureus*, regardless of the residue number (30, 100, or 200) (Fig. 2a). More precisely, PAR30 MIC was about 0.01 mg.mL^{-1}, whereas it was about 0.025 mg.mL^{-1} for PAR100 and PAR200 (Fig. 2a). For PLL and PLO polycations, we observed an antimicrobial activity with a high effectiveness, preventing almost 100 % of pathogen growth at 0.01 mg.mL^{-1} (Fig. 2b and c), regardless of residue numbers in the chains.

To evaluate the effect of PAR, PLL, and PLO polycations against a eukaryotic pathogen, *C. albicans* was selected as a yeast model and similar MIC assays were performed. We observed growth inhibition of *C. albicans* only in presence of higher concentrations (0.5 mg.mL^{-1}) of polycations for all tested chain lengths (PAR with 30, 100, and 200 residues; PLL and PLO with 30, 100, and 250 residues) (Figure S3, S4 and S5).

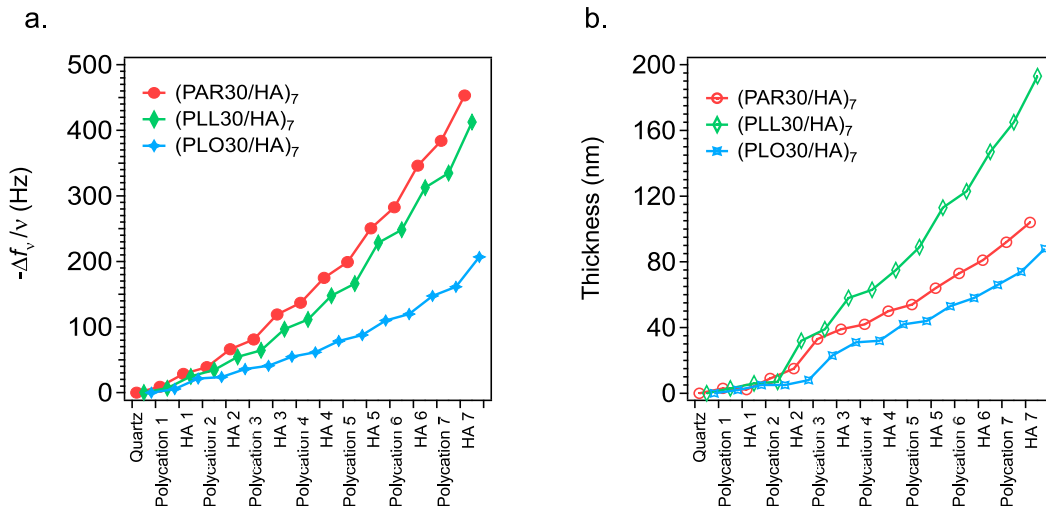In short, PAR, PLL, and PLO polycations effectively prevented

Fig. 1. Construction of (polycation/HA)₇ multilayer films on SiO₂-coated crystal monitored by QCM-D with PAR30 (red), PLL (green), and PLO (blue) as polycations. **a.** Evolution of the normalized frequency $-\Delta f_\nu/\nu$ (for $\nu = 3$) as a function of the number of adsorbed layers is shown. **b.** Evolution of the estimated thickness as a function of adsorbed layers is shown. HA: hyaluronic acid; PAR: poly(L-arginine), PLL: poly(L-lysine), PLO: poly(L-ornithine). (For interpretation of the references to colour in this figure legend, the reader is referred to the Web version of this article.)
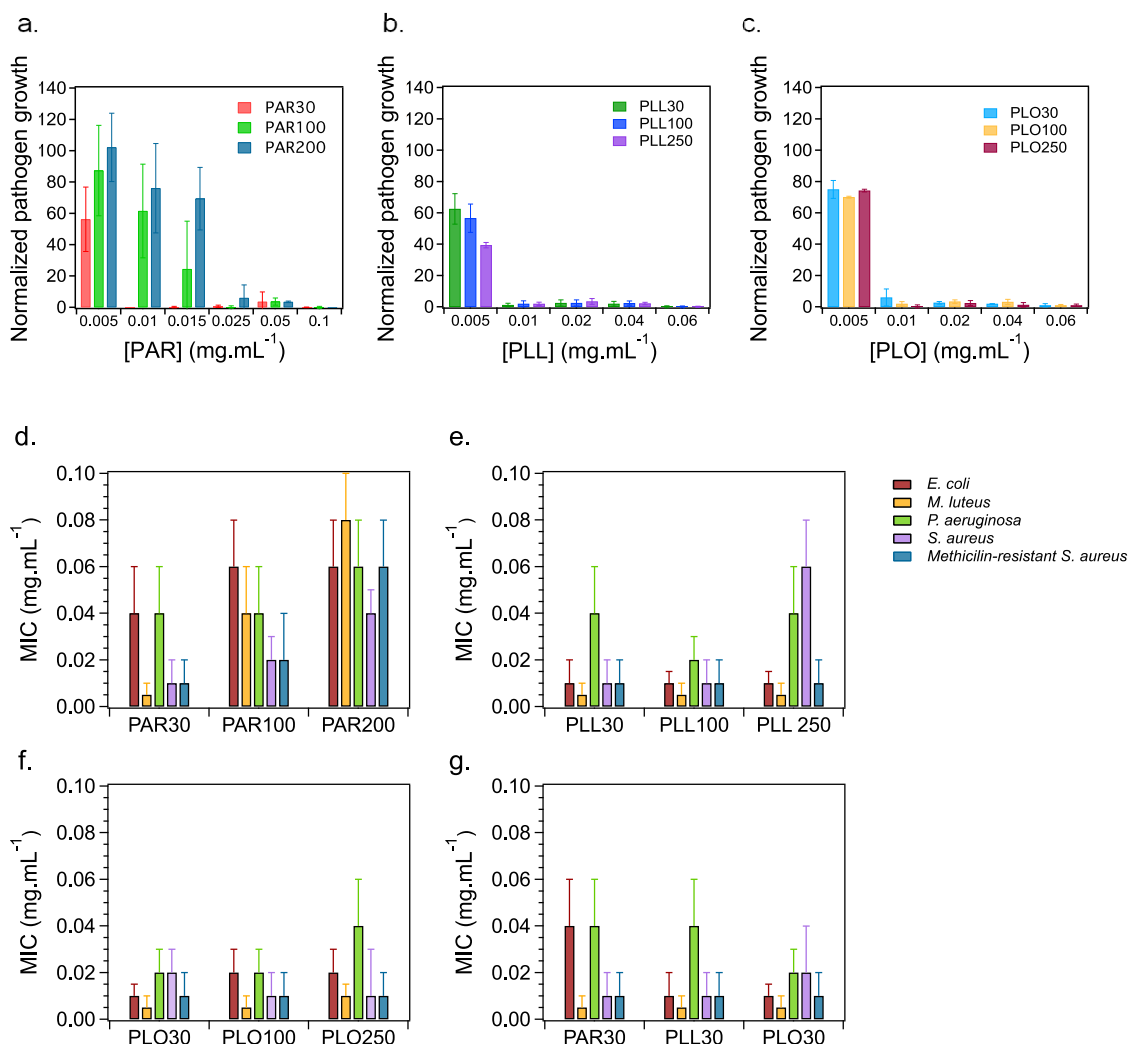
Fig. 2. Normalized pathogen growth of *S. aureus* as a function of polycation concentration (in mg.mL^{-1}) measured in solution with PAR containing 30, 100, and 200 arginine residues **(a)**, with PLL containing 30, 100, and 250 residues **(b)** and with PLO containing 30, 100, and 250 residues **(c)**. Minimal inhibitory concentration (MIC, in mg.mL^{-1}) of *E. coli, M. luteus, P. aeruginosa, S. aureus* and *MRSA* for polycations, measured in solution for PAR with 30, 100, and 200 residues **(d)**, for PLL with 30, 100, and 250 residues **(e)** and or PLO with 30, 100, and 250 residues **(f)**. Comparisons of MIC values with PAR, PLL, and PLO containing 30 residues **(g)**. Each polycation was incubated for 24 h at 37 °C in 300 µL of bacterial culture medium with an initial bacterial concentration corrresponding to OD$_{620}$ = 0.001. Each value corresponds to the mean value of three individual experiments (three samples per experiment and condition). All error bars represent standard deviations. PAR: poly(L-arginine), PLL: poly(L-lysine), PLO: poly(L-ornithine).

S. aureus growth, whereas this effect was lower against a yeast like *C. albicans*. However, these results suggest that these homopolypeptides might be considered as new interesting candidates to efficiently prevent the growth of bacterial pathogens such as *S. aureus*, which is one the

most important bacterium involved in nosocomial infections [5].

We implemented these MIC assays with *E. coli, M. luteus, P. aeruginosa, S. epidermidis,* and *MRSA*. They are involved in nosocomial infections and belong to the ESKAPE pathogens, which are particularly
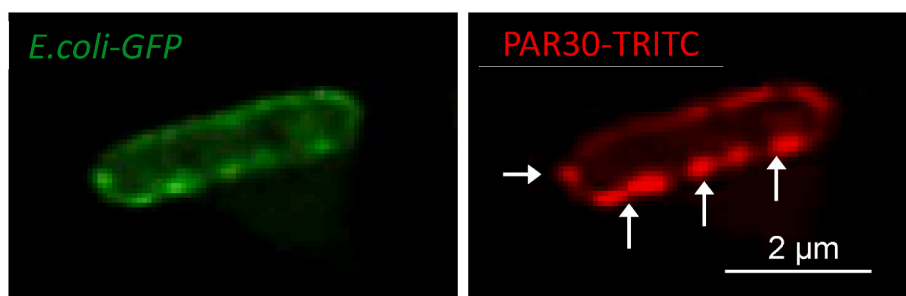

Fig. 3. Localization of PAR30-TRITC in *E. coli*-GFP. High resolution image of *E. coli*-GFP (green channel on the left) and PAR30-TRITC (red channel on the right) with super resolution confocal microscopy. White arrows point a PAR30-TRITC accumulation at membrane of *E. coli*-GFP. GFP: green fluorescent protein, TRITC: tetramethylrhodamine, PAR: poly(L-arginine), GFP: green fluorescent protein. (For interpretation of the references to colour in this figure legend, the reader is referred to the Web version of this article.)

resistant to multidrug treatments [27,37,38]. The results indicated that MICs were less than 0.08 mg.mL^{-1} for PAR, PLL, and PLO for chains having 30 residues or more, suggesting a strong killing activity against all tested pathogens (Fig. 2 d, e, f, g).

3.3. Understanding the mechanism with super resolution microscopy

In order to confirm the antibacterial property of (PAR/HA) coatings via a contact-killing mechanism, we performed super-resolution confocal microscopy with green fluorescent *E. coli* (*E. coli*-GFP) incubated with PAR30 (Fig. 3). These images demonstrated that PAR30 chains, labeled with a red fluorescent dye (TRITC), strongly interacted with the bacteria and were concentrated on bacterial membrane. The accumulation of positively-charged PAR chains (white arrows, Fig. 3) probably destabilized the negatively-charged membrane and caused bacteria lysis. The absence of the PAR30 inside the bacteria demonstrates that the lysis happened faster than PAR30 internalization, and thus presumably avoided any downstream biological effects on DNA for example. This provides for the first time a local view of the antimicrobial mechanism of PAR30 through high-resolution images.

3.4. Antimicrobial activity of homopolypeptide/HA films

After successfully demonstrating the proper assembly of PLL and PLO with HA, as well as confirming their intrinsic antimicrobial properties and the contact killing mechanism of PAR30, the next step evaluated the antimicrobial activity of the polycations within an LbL nanocoating system. *S. aureus* growth in contact with films composed of 24 bilayers of polycations/HA (with 30, 100, and 200, or 250 residues for polycations). While the films containing polycations with 30 residues, *i.e.*, (PAR30/HA)$_{24}$ and (PLL30/HA)$_{24}$, prevented *S. aureus* growth (Fig. 4a and b), the films composed of PAR or PLL chains having 100 or 200 residues (*i.e.*, (PAR100/HA)$_{24}$ and (PAR200/HA)$_{24}$ or (PLL100/HA)$_{24}$ and (PLL200/HA)$_{24}$) did not efficiently inhibit *S. aureus* growth. As a visual confirmation, (PLL/HA)$_{24}$ surfaces were observed by confocal microscopy after 24 h of *S. aureus* incubation (Fig. S6). The images revealed an absence of *S. aureus* bacteria on (PLL30/HA)$_{24}$ films, whereas bacteria were present on glass or films made with PLL100 and PLL250. Additionally, (PLO/HA) films displayed antimicrobial activity with PLO having 30 residues, but also with 100 residues, whereas (PLO250/HA)$_{24}$ did not prevent pathogen growth (Fig. 4c).

To evaluate the broad antimicrobial potential of the investigated nanocoating systems, several pathogens were tested using polycations with coating based on homopolypeptides with 30 residues. Normalized pathogen growth for *S. aureus 25923*, *MRSA*, *E. coli*, *M. luteus*, and *P. aeruginosa* confirmed the antimicrobial activity for the multilayer films built with cationic homopolypeptides PAR, PLL, and PLO containing 30 residues (Fig. 4d). The (polycation30/HA)$_{24}$ films specifically prevented the growth of a broad prokaryotic target (Fig. 4d). However, the coating did not prevent *C. albicans* growth, a eukaryotic pathogen (Fig. S7), which is in line with the absence of activity against *C. albicans* previously observed with polycations in solution (Fig. S3).

The number of layers constituting the coating is probably also a key parameter and series of experiments with 6, 12 and 24 bilayers were
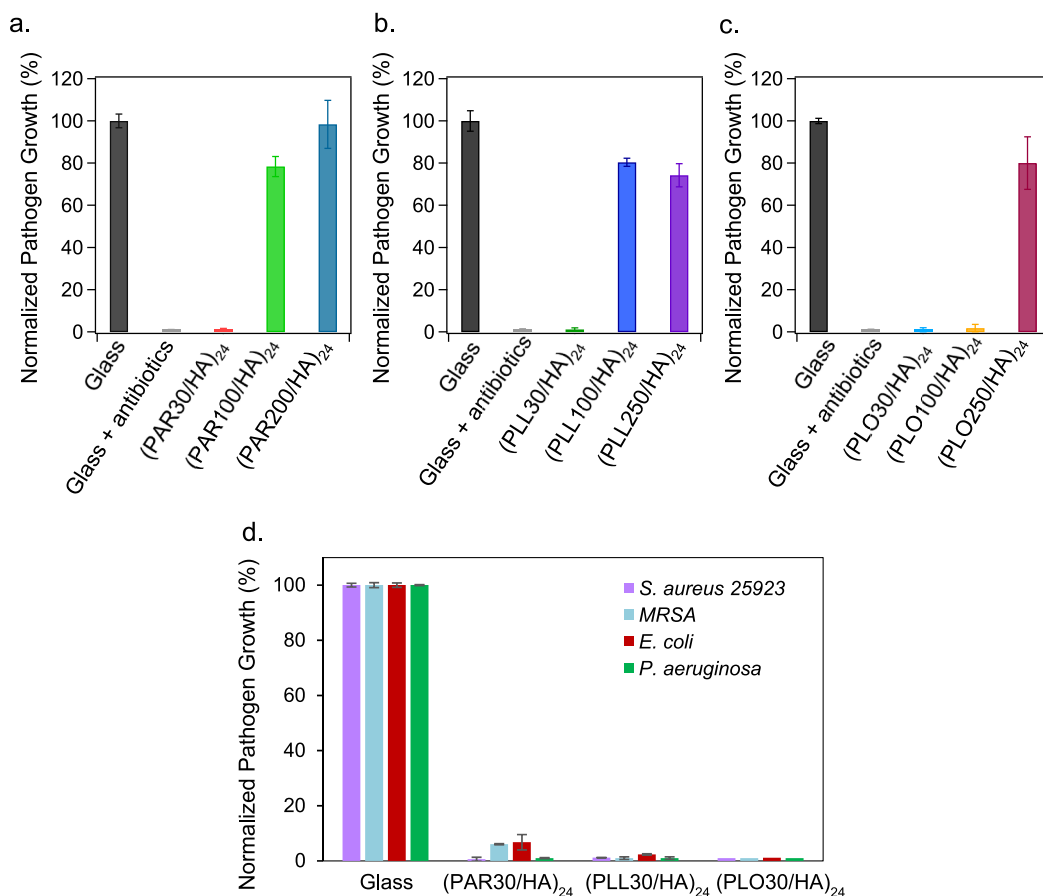

Fig. 4. Normalized *S. aureus* growth in supernatant after 24 h in contact with (polycation/HA)$_{24}$ multilayer films PAR **(a)**, PLL **(b)**, and PLO **(c)** with a variable number of residues per chain. Normalized pathogen growth (*S. aureus, MRSA, E. coli, P. aeruginosa*) in supernatant after 24 h in contact with (polycation30/HA)$_{24}$ **(d)**. Each (polycation/HA)$_{24}$ multilayer films was incubated for 24 h at 37 °C in 300 μL of bacterial culture medium with an initial bacterial concentration correspondinf to OD$_{620}$ = 0.001. PAR: poly(ʟ-arginine), HA: hyaluronic acid, PLL: poly(ʟ-lysine), PLO: poly(ʟ-ornithine), MRSA: methicillin-resistant *Staphylococcus aureus*.

performed to determine the influence of this parameter on the activity (Fig. S8).

3.5. Mobility of homopolypeptide chains in the films

In our previous study, the antimicrobial activity of PAR30 in the multilayer film (PAR30/HA)$_{24}$ was related to the high PAR mobility in the film [17]. To confirm the hypothesis that the mechanism was the same for films built with PLL and PLO chains with 30 residues, fluorescence recovery after photobleaching (FRAP) experiments were performed on (polycation30/HA)$_{24}$ films (Fig. 5a and b). As expected, a high normalized fluorescence recovery after photobleaching was obtained with films built with PLL30 and PLO30 polycations, close to the recovery of PAR30 chains (Fig. 5a). Based on three independent experiments, the mobile PAR30, PLL30, and PLO30 proportions in the films were evaluated. In all conditions, about 90 % of chains were mobile (Fig. 5b). These results suggest a contact-killing mechanism for PLL30 and PLO30, similar to that previously described for (PAR30/HA)$_{24}$ [18].

To sum up, PLL30 and PLO30 self-assembled with HA in nanocoating systems presented a similar behavior to that of PAR30 in terms of the physical properties, suggesting some general rules emphasizing the importance of the mobility of the polycation inside the multilayer films.

3.6. Biocompatibility of homopolypetide/HA films and NO release from PAR30/HA films

To minimize complications associated with implants (for instance chronic inflammation or tissue necrosis) and guarantee long-term durability, the biocompatibility of implant coatings is one of the main parameters to evaluate. Here, we investigated the biocompatibility of our nanocoating systems by evaluating cell viability, adhesion, and proliferation on different cell lines: fibroblasts, epithelial and endothelial cells.

First, cytotoxicity tests were performed using fibroblast cells (Balb/3T3), as they are one of the recommended cell lines in the ISO 10993:5 norm for initial evaluation of material toxicity. The extraction medium, composed of the culture medium in contact for 24 h with the (polycation30/HA)$_{24}$ films, was diluted at 12.5 %, 25 %, 50 %, and 100 % in fresh culture medium and added to fibroblast monolayers. After 24 h of

seeding, cell metabolic activity was evaluated (Fig. 6a). For the extraction media originating from (PAR30/HA)$_{24}$ and (PLL30/HA)$_{24}$, metabolic activity was more than 70 % (violet line, Fig. 6a) for all conditions (diluted medium of 12.5 %, 25 %, 50 %, and 100 %) compared with the metabolic activity obtained with fresh medium (100 %, prior incubation with any coating), indicating the absence of cytotoxicity of these coatings according to the ISO 10993:5 standard. For cells cultured with diluted medium extracted from (PLO30/HA)$_{24}$, a high metabolic activity for 12.5 % and 25 % dilutions was observed. However, in the presence of 50 % and 100 % of extraction medium, significant cytotoxicity was monitored, with a metabolic activity decrease of about 40 % and 80 %, respectively (Fig. 6a).

Despite the absence of cytotoxicity in fibroblasts exposed to the extracted medium in contact with (PLL30/HA)$_{24}$ (Fig. 6a), previous studies have shown that cells exhibited poor spreading, weak adhesion, and limited proliferation on the (PLL30/HA)$_{24}$ coating [39,40]. This problem related to the coating softness can be resolved by a crosslinking of the multilayers with EDC/NHS (N-Ethyl-N′-(3-(dimethylamino)propyl)carbodiimide hydrochloride/N-Hydroxysuccinimide) or other crosslinking systems [41,42]. However, crosslinking involves a significant change in the coating properties. Indeed, when polycationic chains are crosslinked, their mobility is strongly reduced, which significantly decreases the antimicrobial activity, as suggested in our former study with (PAR/HA) coating [17]. Therefore, the next adhesion experiments were performed without (PLL/HA) coatings, and we focused on (PLO/HA) and (PAR/HA) coatings without crosslinking, as there were no previous data on these coatings about cell adhesion. To monitor cell adhesion at high resolution, we used MDCK epithelial cells as a cell adhesion model and we evaluated their adhesion using AFM (Fig. 6b). MDCK cells were well spread and exhibited a healthy cellular monolayer on (PAR30/HA)$_{24}$, similar to the monolayer observed on the glass substrate. In contrast, (PLO30/HA)$_{24}$ coatings displayed only a limited number of unhealthy cells (Fig. 6b). High resolution images with SEM were also obtained on the (PAR30/HA)$_{24}$ coating (Fig. S9). These fine resolution images confirmed the spreading and adhesion of epithelial cells on the (PAR30/HA)$_{24}$ film. Moreover, immunofluorescence images confirm the adhesion of cells on (PAR30/HA)$_{24}$ film with formation of vinculin spots and stress fibers. By comparison, the adhesion on (PLO30/HA)$_{24}$ is weak and no vinculin spots and stress fibers were clearly observed (Fig. S10). In conclusion, epithelial cells successfully
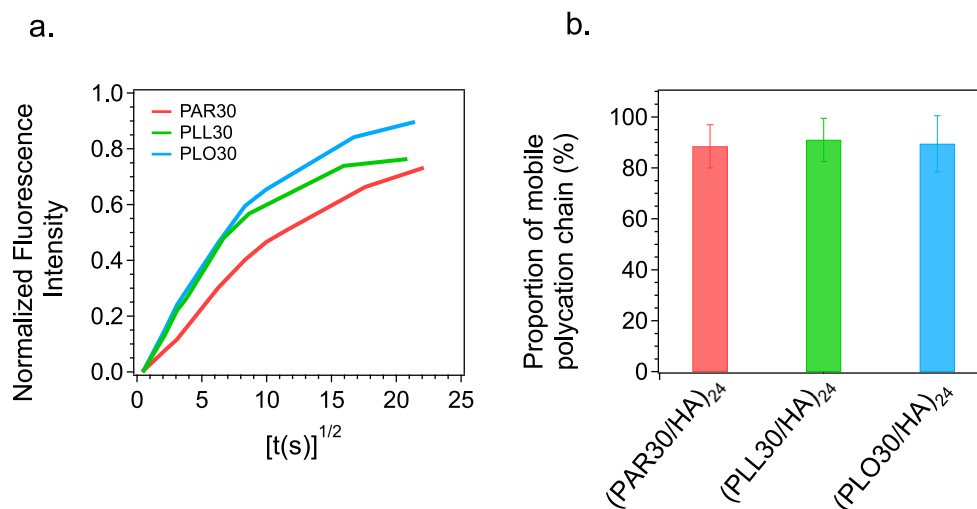

Fig. 5. Characterization of the mobility of polycation inside the multilayer films. **a.** Normalized fluorescence intensity recovery in a photobleached area as a function of $[t]^{1/2}$ for each (polycation-FITC/HA)$_{24}$ film, with PAR30 (red), PLL30 (green), and PLO30 (blue) as polycations. $t = 0$ corresponds to the end of the photobleaching step. A typical experiment per polycation is shown. **b.** Corresponding proportion of mobile polycation chain derived from data in part. Three independent experiments for each polycation were performed and error bars correspond to standard deviations. PAR: poly(ʟ-arginine), PLL: poly(ʟ-lysine), PLO: poly(ʟ-ornithine). (For interpretation of the references to colour in this figure legend, the reader is referred to the Web version of this article.)
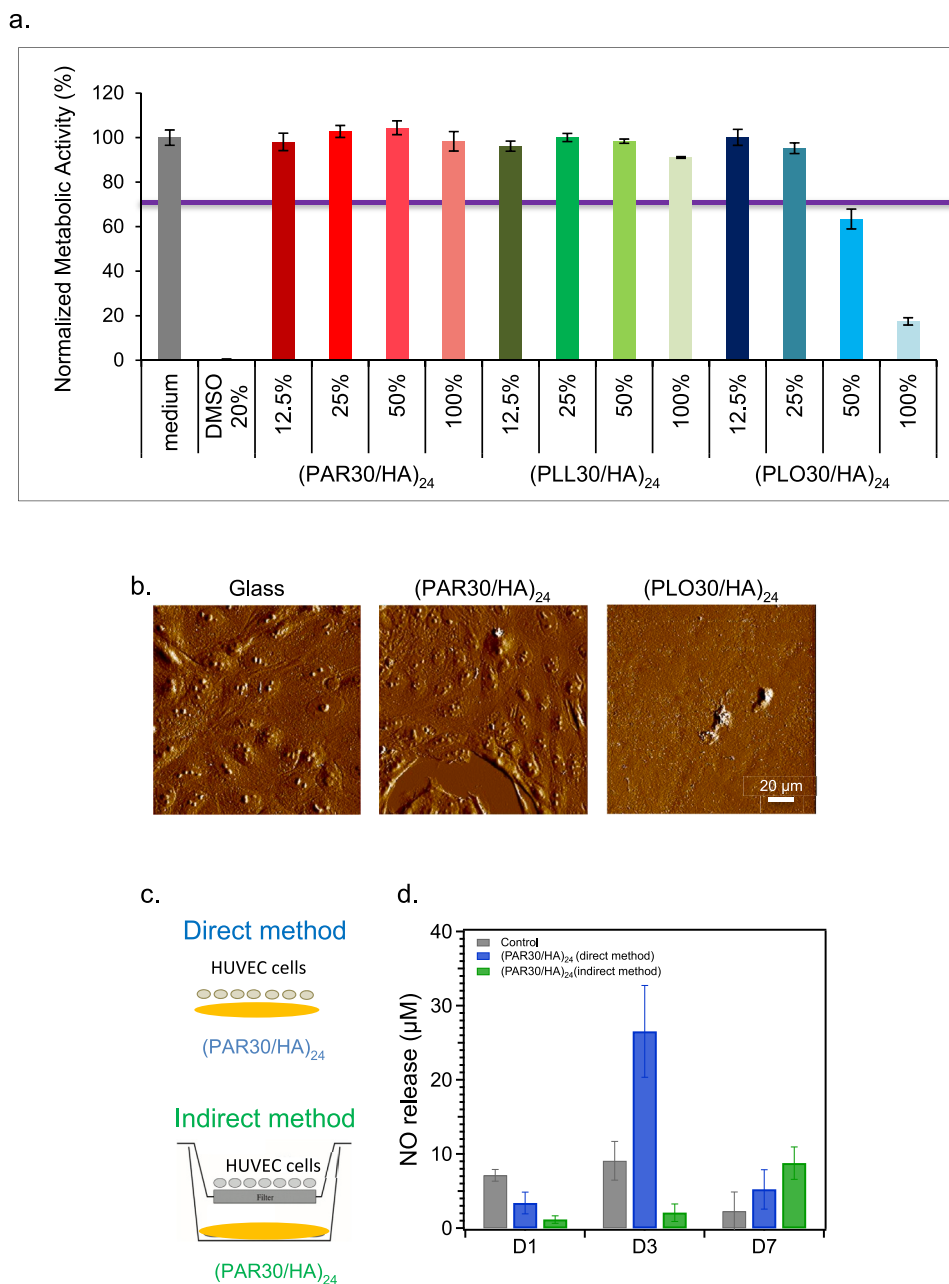
Fig. 6. Cytotoxicity assays, cell adhesion assays, and NO release quantification. **a.** Metabolic activity of Balb/3T3 cells incubated for 24 h with supernatant medium extracts from polyelectrolyte multilayer films in contacts during 24 h. Balb/3T3 cells were cultured in presence of different rates of extraction medium in contact with (PAR30/HA)$_{24}$, (PLO30/HA)$_{24}$, and (PLL30/HA)$_{24}$. Normalized metabolic activity higher than 70 % (violet line) indicates the absence of cytotoxicity in the corresponding solutions. **b.** Deflection AFM images taken in air of epithelial MDCK cells that were cultured on glass, (PAR30/HA)$_{24}$ and (PLO30/HA)$_{24}$ multilayer films. **c.** Schematic representation of the experimental condition, with cells directly in contact with the coating (PAR30/HA)$_{24}$) and cells with no contact with (PAR30/HA)$_{24}$ (right). **d.** NO level quantified through the detection of nitrite in the supernatant in HUVEC. The supernatant was analyzed after 1, 3, and 7 days of culture and mean NO release was obtained from three independent experiments. Error bars correspond to standard deviations. NO: nitric oxide, DMSO: dimethyl sulfoxide, PAR: poly(L-arginine), HA: hyaluronic acid, PLL: poly(L-lysine), PLO: poly(L-ornithine); HUVEC: human umbilical vein endothelial cell, AFM: atomic force microscopy, MDCK: Madin-Darby canine kidney. (For interpretation of the references to colour in this figure legend, the reader is referred to the Web version of this article.)

formed a physiological monolayer across the entire surface of the (PAR30/HA)$_{24}$ coating. This can be particularly interesting in the case of coatings used for wound healing with medical dressings [43,44].

Furthermore, one of the key challenges in the design of biomaterials for tissue regeneration (implants, scaffolds) is angiogenesis promotion [45–47]. This angiogenic capacity can be measured through NO production assessment. Indeed, NO release plays a critical role in maintaining tissue homeostasis and vascular microenvironment [48,49]. Supplementary cell culture assays were carried out, specifically on

HUVECs, to assess their ability to produce NO when exposed to the (PAR30/HA)$_{24}$ coating [50]. In our case, the nanocoating system (PAR30/HA)$_{24}$, through PAR presence, was potentially able to induce angiogenesis. Indeed, arginine is involved in the metabolic pathways and especially in inducible nitric oxide synthase (iNOS) activation, which promotes NO production [51]. NO production was monitored with HUVECs seeded either directly on the (PAR30/HA)$_{24}$ films (direct method) or in a cell culture insert above the (PAR30/HA)$_{24}$ coating deposited at the bottom of the plate (indirect method) (Fig. 6c). We

observed a strong NO production by HUVECs directly seeded on (PAR30/HA)$_{24}$ at day 3, corresponding to a threefold increase compared with the control surface (without any coating) (Fig. 6b). Cells in indirect contact with the coating were stimulated later, during the 7th day instead of the 3rd day for direct seeding. This result suggests that the nanocoating system (PAR30/HA)$_{24}$ stimulated NO production, which, in the presence of PAR, might be attributed to the fact that arginine is the main NO synthesis precursor [52–54]. The NO production delay between direct and indirect methods (Fig. 6a) could be attributed to the kinetic of PAR absorption by the cells. In the indirect method, PAR release and diffusion in the cell culture media are required before the NO synthesis process can be initiated. This diffusion route may contribute to the observed delay in NO production compared with the direct method [55].

Finally, the nanocoating system (PAR30/HA) emerged as the best candidate as an LbL coating because of its ability to fight against prokaryotic cells, therefore preventing bacterial infections, while being biocompatible for eukaryotic cells. Indeed, this coating presented interesting cumulative biocompatibility properties, such as the maintenance of fibroblast proliferation and epithelial cell adhesion (and consequently the formation of an epithelial monolayer). Furthermore, the PAR-based coating promoted NO generation, which contributes to favor the angiogenesis mechanism [56,57]. These results emphasize the use of the (PAR/HA) LbL nanocoating in medical applications for the prevention of nosocomial infections and the improvement of the integration of coated implants after surgery implantation.

3.7. Evaluation of PAR30/HA coating antibacterial activities through ISO standard methods

To confirm the activity of the (PAR30/HA) coating against several pathogens, we quantitatively evaluated bacteria and yeast growth after 24 h in contact with the (PAR30/HA) coating using the ISO 22196 standard method for assessing antibacterial activity of surfaces. This method is very sensitive and can detect low levels of antimicrobial activity of coatings. After 24 h of bacteria inoculation on surfaces, supernatants were removed from the surfaces and cultured for another 24 h before CFU.mL^{-1} determination. Gram-positive bacteria, *S. epidermidis*, *S. aureus*, *MRSA* and *E. faecalis* were strongly inhibited in the presence of the (PAR30/HA)$_{24}$ coating, as compared to non-coated surfaces (bare glass), with a decrease of about 6 log units in CFU.mL^{-1} (Fig. 7). The Gram-negative bacteria *E. coli* and *P. aeruginosa* and the yeast *C. albicans* were inhibited in a limited way by (PAR30/HA)$_{24}$, with a decrease of 1–2 log units in CFU.mL^{-1}. This could be explained by the amount of PAR30 inside the nanocoating system, which may be insufficient to strongly prevent bacterial growth, in particular Gram-negative bacteria. Thus, we tested a thicker coating built with 48 bilayers instead of 24,

resulting in a (PAR30/HA)$_{48}$ film (Fig. 7). Interestingly, Gram-negative bacteria inhibition became very strong with decreases of about 8 log units for *E. coli* and *P. aeruginosa,* and even about 6 log units for the yeast *C. albicans*. This offers a great perspective in defense strategies against specific targets, such as prokaryotes or eukaryotes in the case of yeast, and shows that coating activity can easily be tuned by adjusting the number of bilayers forming the film.

3.8. Stability of the (PAR30/HA) coating

First of all, it should be borne in mind that the aim of our study was to apply a coating capable of preventing infections, particularly those linked to surgery during implantation of medical devices. This requires to avoid contamination of the medical device during the first hours post-implantation. Our coatings have been designed with this in mind, *i.e.* stability of the coating must be ensured for a short delay (few hours) and thus biopolymers met these expectations.

The first stability study was performed by incubation of (PAR/HA30)$_{24}$ coatings 1, 2 or 7 days in cell culture medium (EMEM, Eagle's minimum essential medium from ATCC) (Figs. S11a–c). Then, *S. aureus* growth in supernatant after 24 h in contact with these (PAR30/HA)$_{24}$ multilayer films was monitored. Antibacterial activity of the films was unchanged, with a total inhibition. Moreover, similar experiments done with pre-incubation with EMEM and FBS (fetal bovine serum) at 2 % show similar results, *i.e.* no loss of antibacterial activity (Fig. S11d). These results suggest that the coating are stable in cell media with or without serum. Moreover, confocal microscopy observations show that in EMEM without FBS, no degradation of the (PAR30^{FITC}/HA)$_{24}$ coating was monitored (Figs. S12a and b). Only a partial degradation of the coating in the presence of serum can be observed, which is probably related to the presence of proteases in this medium (Figs. S12b and c). However, the amount of coating remains sufficient after 24 h to assure an antimicrobial activity.

A second set of experiments to assess the coating stability was performed by using ageing methods (Fig. S13). The (PAR30/HA)$_{24}$ coatings were produced and then they were sterilized by steam-sterilized with a solid cycle at 121 °C for 20 min. Then, they were stored at room temperature for 24 months (Fig. S13b) or by accelerated ageing method for 10 years (Fig. S13c) (using ASTM F1980-16 standard, « Standard Guide for Accelerated Aging of Sterile Barrier Systems for Medical Devices »). After these storage times, antibacterial activity monitored for 24 h with *S. aureus* was maintained, demonstrating the long-term stability of the coating.

A last test was performed by incubating *S. aureus* on a (PAR30/HA)$_{24}$ coatings for 8 days (Fig. S13a). Control experiments with glass surfaces without any coating show a large number of bacteria to the opposite of the coated glasses where no bacteria were monitored after 8 days of
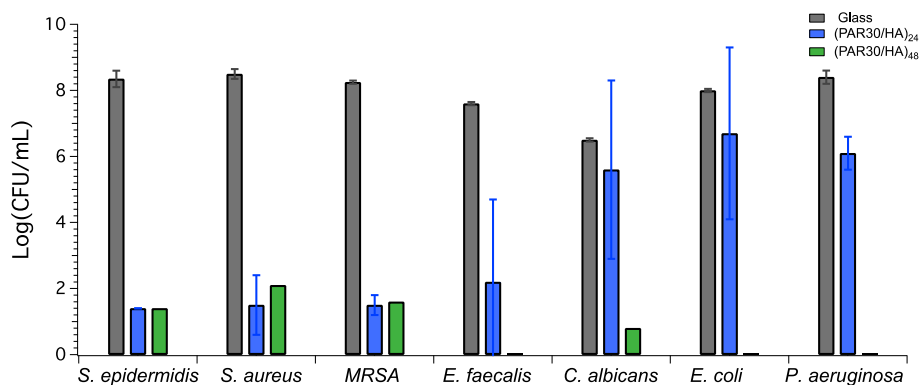

Fig. 7. Pathogens growth evaluated by CFU number after 24 h in contact with (PAR30/HA)$_{24}$ and (PAR30/HA)$_{48}$ multilayer films following the ISO 22196 method. The mean of three independent experiments is shown, error bars correspond to standard deviations. CFU: colony forming unit, PAR: poly(L-arginine), HA: hyaluronic acid.

incubation. This impressive result suggest again that the coating is very stable in growth media.

3.9. Absence of direct induction of bacterial resistance to PAR30 homopolypeptide

From the results obtained above, the (PAR30/HA) coating appeared as the "hit" system for preventing bacterial infections while maintaining good biocompatibility and even tissue regeneration. To go deeper into the characterization and validation of the potential of this coating, we performed complementary tests. Many bacteria use resistance strategies to overcome antibiotics, and this is probably the leading cause for the rise of infections [58,59]. Thus, designing new coatings based on biopolymers was certainly a promising strategy, but it was necessary to verify that the antimicrobial polycation itself did not induce resistance behavior in bacteria. For this purpose, a resistance acquisition assay with *S. aureus* to PAR30 was performed. The *S. aureus* strain was inoculated every day during 30 days at a concentration of 10^6 CFU.mL^{-1} and in the presence of a concentration of half of PAR30's MIC. MIC values were evaluated every 3–4 days and PAR30 and tetracycline solutions were adjusted accordingly. The fold changes of the MIC values compared with the initial MICs are reported in Fig. 8. A conventional antibiotic (tetracycline) was used as a reference following the same protocol [60]. As shown in Fig. 8, no relative PAR30 MIC increase was observed over the 30 days of the experiment, whereas the relative MIC for tetracycline increased by more than 50-fold (Fig. 8).

This highlights the strong potential of PAR30 as a privileged tool in the fight against bacteria, and even more against bacteria developing resistance to conventional antibiotics like tetracycline. A second resistance assay was performed by maintaining PAR and tetracycline concentration constants over time (half of the initial MIC). The results demonstrated that the relative MIC was strongly stable over the growth of bacterial generations, whereas the relative MIC for tetracycline increased by around 3 times (Fig. S14). The resistance increase developed by *S. aureus* against tetracycline seemed to be lower when using the second protocol compared with the previous method described in Fig. 8. This difference probably originates from the fact that the PAR and
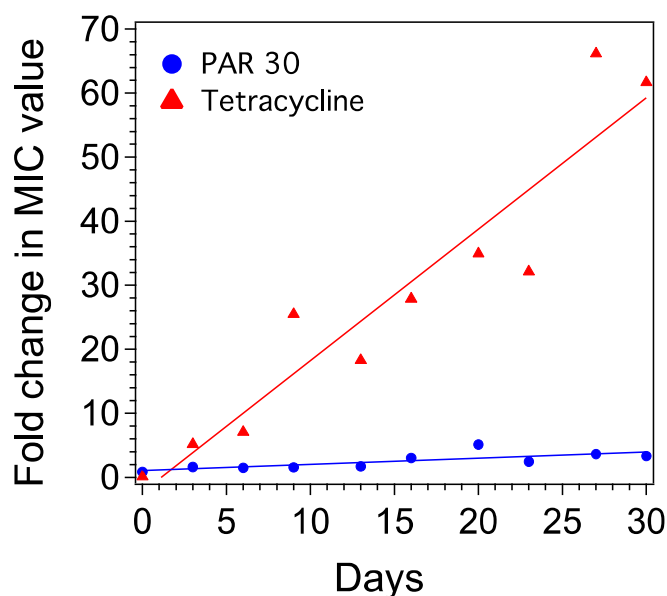

Fig. 8. Resistance acquisition assay of *S. aureus*. *S. aureus* were cultured in the presence of half of the MIC of the antibacterial agent (PAR30 and tetracycline, a conventional antibiotic) for 30 days. The fold changes of MIC values compared with the initial MICs were evaluated at the indicated days and the PAR30 and tetracycline solutions were adjusted accordingly. MIC: minimal inhibitory concentration, PAR: poly(ʟ-arginine).

tetracycline solutions were adjusted to half of the MIC throughout the experiments in the first method (Fig. 8). Although the first method considered MIC variations after each passage and emphasized the resistance of the pathogen against tetracycline, both methods go in the same direction and clearly suggest the absence of bacterial resistance induction against PAR30.

3.10. In vivo evaluation of the PAR30/HA coating on hernia surgical meshes

Hernia surgery is the most commonly performed operation over the world, with more than 20 million hernia repairs each year [26]. Technique selection for hernia repair is mainly based on prosthetic options and especially mesh fixation [61]. However, 60 000 repairs fail each year due to mesh infections [26]. Using meshes containing anti-infective agents released locally in an effective way is the expected solution. For this purpose, we conducted an *in vivo* study to determine whether the composition of the antimicrobial polymer coatings based on (PAR30/HA) could prevent bacterial colonization of the mesh applied in hernia surgery. We achieved this by using a rabbit model infected with *S. aureus* following the protocol established by Fernández-Gutiérrez et al. [30]. The hernia repair material used was Optilene Mesh Elastic [62] (B. Braun, Melsungen, Germany) made of polypropylene (Fig. S1a). First of all, we checked that the (PAR30/HA)$_{24}$ coating can be deposited on polypropylene surface. QCM experiments were performed with quartz crystal coated with polypropylene (Fig. S15). This shows that the step-by-step deposition leads to an increase of frequency after each deposition step. It suggests that the film is built up layer by layer in the right way, as on SiO$_2$ coated-crystals. Moreover, the antibacterial activity was assessed *in vitro* on these polypropylene meshes coated with 24 or 48 bilayers of PAR30/HA (Fig. S16) and a total bacterial growth inhibition was observed.

For *in vivo* studies, three conditions were studied with seven rabbits per group: *group #1* meshes without any coating as a control group; *group #2* meshes coated with (PAR30/HA)$_{24}$; and group #3 meshes soaked in aqueous 0.05 % CHX, a conventional protocol used by some surgeons.

To test the antimicrobial efficiency of the coated meshes, a 0.25 mL inoculation of *S. aureus* ($1–1.5 \times 10^6$) was injected on the surgical defect before mesh fixation with polypropylene sutures on the lateral side of the abdominal wall. Then, the skin tissue was closed by simple interrupted stitches with a 3/0 silk suture (Fig. S1b).

3.10.1. Postoperative follow-up

From the day of the surgery and during the entire study period (14 days), all animals were daily checked to capture any relevant macroscopic and behavioral findings related to the bacterial infection and/or post-surgical complications. No mortality was recorded. Overall, animals from the different study groups behaved similarly in terms of movement, physical activity, and food/drink intake. An expected weight loss was recorded during the first postoperative week (Fig. S17). These recordings were made under normal parameters (about 1–6%) in all groups. Most animals gradually regained their original weight at the end of the study.

3.10.2. Scoring of macroscopic observations and bacterial colonization on the meshes

At necropsy, all animals were subjected to a complete examination to score the most relevant macroscopic observations for each specimen, not only regarding the contaminated meshes, but also in the surrounding tissues (Fig. 9). Upon physical examination, soft-to-touch bulges were observed under the skin of some animals. In general, these bulges were macroscopically evidenced during the second postoperative week. For group #1 (animals with meshes without coating and treatment), none of the animals developed skin fistula or necrosis, although edematous areas were observed in one specimen (Fig. 9a). Meshes were encapsulated in a
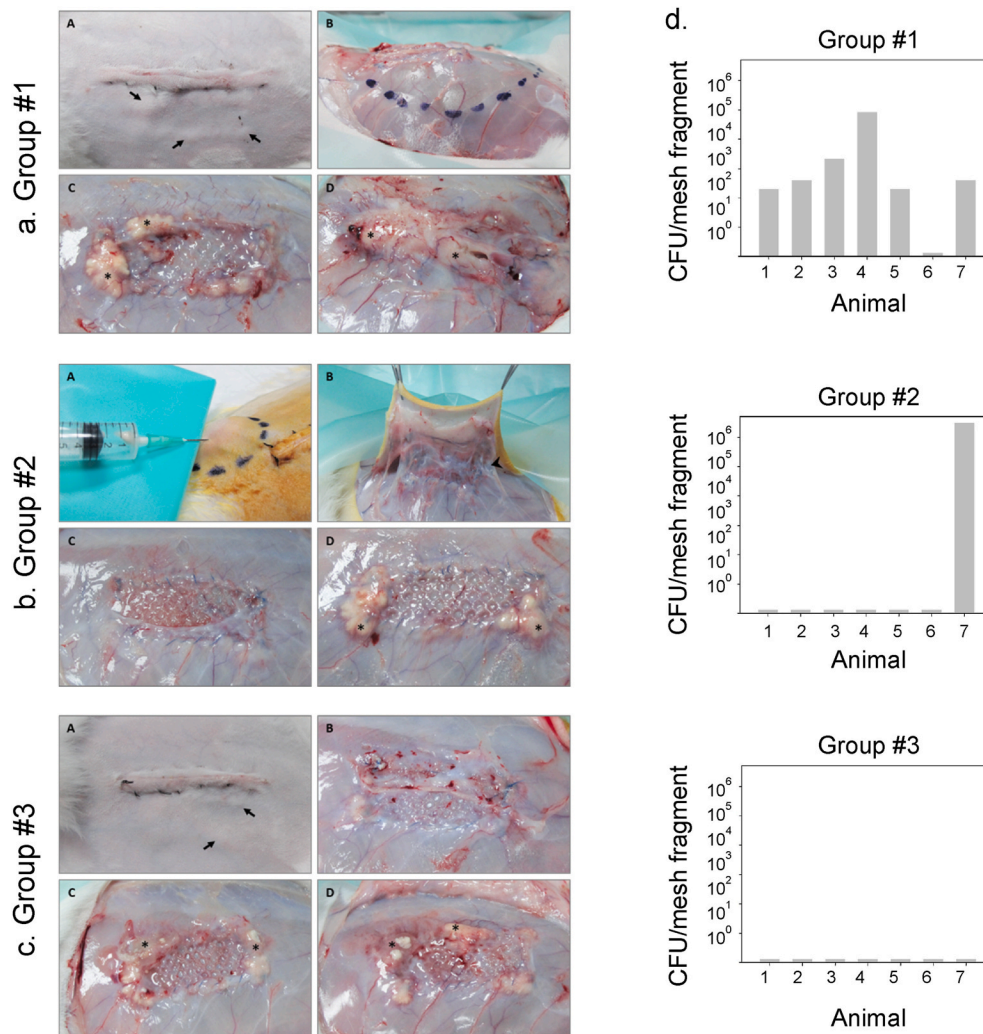
Fig. 9. Macroscopic outcomes of different implants at euthanasia and quantification of bacteria adhesion on the implants. **a**. Group #1, (A) Evidence of discrete bulges (arrows) developed under the skin tissue. (B) Implant showing an edematous swelling (dashed line). (C) Implant partially covered by purulent material (*). (D) Implant with severe vascularization and fully covered by purulent material (*). **b.** Group #2, (A) Evidence of a subcutaneous abscess (dashed line) containing solid purulent material. (B) Detail of a thin fibrous capsule (arrowhead) surrounding an implant. (C) Implant surface with no macroscopic evidence of infection. (D) Implant showing dispersed purulent material (*) restricted to the areas of mesh anchorage. **c.** Group #3 (A) Evidence of discrete bulges (arrows) developed under the skin tissue. (B) Implant surface with no macroscopic evidence of infection. (C, D) Implants showing dispersed purulent material (*) restricted to the areas of mesh anchorage. **d.** Quantification of bacterial adhesion to the surface of central mesh fragments collected from the different implants for each animal in each group. CFU: colony forming unit.

moderate to thick fibrous capsule and displayed different amounts of purulent material distributed along the implant surface. In areas of the implant exhibiting purulent material, the mesh was partially integrated into the host tissue. A moderate hypervascularization of the implant surface was recorded in almost all specimens, and hematoma signs were observed in one specimen. Group #2 (meshes coated with (PAR30/HA)$_{24}$) showed no development of skin fistula, necrosis, or edema (Fig. 9b). Moreover, meshes were surrounded by a thin fibrous capsule and presented good tissue integration, which exhibited a large abscess covering part of the mesh. Presence of purulent material was observed but associated with mesh anchorage areas (suture line). Hypervascularization was less intense in this group compared with control implants. In general, implants displayed good tissue integration. In group #3 (animals with meshes treated with aqueous 0.05 % CHX solution dipping), no animal developed skin fistula, necrosis, or edema. Macroscopic observations from this group were similar to those observed in many specimens from group #2. In these implants, meshes were surrounded by a thin fibrous capsule. Some specimens exhibited presence of purulent material in association with the suture line.

Hypervascularization was less intense in this group compared with control implants (Fig. 9c).

Finally, group#1 presented more purulent material, strong hypervascularization, moderate to severe fibrous capsule, and weak tissue integration. Specimens exposed to meshes coated with (PAR30/HA)$_{24}$ presented very similar observations to that of specimens with meshes treated with aqueous 0.05 % CHX, which were less purulent material, weak hypervascularization, and better tissue integration. Thus, to go dipper than macroscopic observations, the next approach was based on the evaluation of bacterial infection on the meshes.

To determine the bacterial load adhered to the meshes, tissue explants containing a mesh fragment (2×1 cm^2 each) from each animal included in the three study groups were used to perform bacterial recovery assays. Samples were collected from the cranial border (lateral and central fragment) after host tissue removal (Fig. S1c). Following sonication, supernatant plating, and incubation, colonies were counted. Due to the macroscopic observations concerning purulent material localization, the hypothesis that the suture line was the source of the infection was strengthened. Thus, only the central fragments of the

explanted meshes, where suture line infections did not interfere much, were considered to determine the number of viable bacteria adhered to the surface (Fig. 9d). In control group #1, all animals presented infections except one. The coating applied in group #2 clearly prevented infections, as only one animal had bacteria while the six others displayed no infection signs. CHX solution appeared clearly as the most powerful treatment as no animals were infected (Fig. 9d).

3.10.3. Histological evaluation and cytotoxicity test

To deeply analyze the state of the tissues surrounding the implant, we performed histological experiments. Tissue explants were processed according to the methodology described in the materials and methods section and observed under optical and electronic microscopes. For group #1, mesh filaments were surrounded by a dense neoformed connective tissue which infiltrated the pores in a concentric fashion (Fig. 10a). The tissue displayed barriers of inflammatory and foreign-body giant cells in peri-prosthetic areas, as well as tissue exudate accumulation (see C1858, C1864, and C1865 in Fig. S17) and large abscesses (C1865, C1877, and C1882). Abscesses were mainly located close to the implant borders and contained debris, inflammatory cells, and bacteria (Fig. 10a and S17). Mesh integration was only altered in areas of the neoformed tissue adjacent to the abscesses. Bacteria presence on the implant was acute within the abscesses and more discrete along the neoformed connective tissues (Fig. 10a). Meshes from group #2 (coated with (PAR30/HA$_{24}$)) were surrounded by neoformed connective tissues looser than those observed in the uncoated control implants (Fig. 10b). Peri-prosthetic inflammatory cells and tissue exudate accumulation (C1859 and C1867) were also recorded (Fig. S18). In these implants, either micro- (C1849, C1862) and macroabscesses (C1859, C1880) were embedded along the neoformed tissue in a dispersed fashion (Fig. S18). Overall, these structures were smaller than those developed in control implants, although the largest ones also disrupted mesh integration into the host tissue. Bacteria were especially observed within the abscesses, but with a smaller amount than that observed in the control group (Fig. 10b and S18). Regarding the last group, histological observations were similar to those recorded in group #2. Meshes were surrounded by a loose neoformed connective tissue which infiltrated the pores, allowing adequate tissue integration of the implants (Fig. 10c). Tissue exudate accumulation was found in some implants (C1861 and C1881) and two specimens developed either micro- (C1878) or macroabscesses (C1881) (Fig. S19). A moderate inflammatory reaction caused by CHX addition was also highlighted (Fig. S19). In the neoformed connective tissue, bacteria presence was not recorded or noticeably reduced compared with the other experimental groups (Fig. 10c).

Histological analyses confirmed the good integration in the tissue of coated meshes and meshes dipped in CHX solution. Bacteria presence was noticed mostly for the untreated group, suggesting that using a (PAR30/HA)$_{24}$ coating is comparable in terms of infection prevention to a dipping step of the implant in CHX before implantation. Moreover, no chronic inflammation was observed for all tested groups. This observation was confirmed by the evaluation of systemic cytokine levels using ELISA assays targeting most of the common inflammatory cytokines (TNF-α, IFN-γ, Il-10, and IL-6). ELISA results for all tested cytokines on the plasmatic levels did not present any significative difference before and after surgery of animals (Fig. S20).

While CHX was already known to be cytotoxic [63], we performed new tests with the same protocol as the one used for (PAR/HA)$_{24}$ coating, to confirm the unwanted effect of CHX on the cells. Tests were performed with CHX in solution in the presence of fibroblasts, following ISO 10993-5 standard which specifies test methods for evaluating the *in vitro* cytotoxicity of medical devices (Fig. S21). For CHX concentrations ranging from 0.02 to 0.5 mg.mL^{-1}, a high toxicity degree was observed with cell viability values lower than 30 %, far from the 70 % of viability required to pass the test (Fig. S21). This confirms that CHX as a biocide, possesses strong antibacterial properties, is a cytotoxic compound, and

that high doses adsorbed on the mesh can negatively impact healthy tissues surrounding the implantation site.

4. Conclusion

The design of effective antimicrobial coating systems is one of the strategies to be developed to combat pathogen infections related to medical devices, which represent about 50 % of hospital-acquired infections. In this study, we demonstrated the strong antimicrobial activity of coatings based on 24 bilayers composed of PAR, PLL, and PLO self-assembled with HA against relevant bacteria involved in nosocomial infections. System efficacy was tuned with the increase of (polycation/polyanion) bilayer number, providing an effective nanocoating system on the device to prevent the growth of prokaryotic pathogens, but also eukaryotic pathogens like yeast. Finally, the mobility of the selected polycations in the coating was critical to ensure antimicrobial properties due to the contact-killing mechanism involved. The mechanism included the interaction of PAR30 with the pathogen membrane, initiating the killing process. The (PAR30/HA)$_{24}$ film provided an optimal antimicrobial activity without perturbing host mammalian cell activity and cell adhesion, allowing different cell types to deploy their original functions. The nanocoating systems studied in this work showed that we can personalize coatings not only by adjusting the layer number, but also by modulating the polycation nature. For example, depending on the needs (if the device surface needs to be adhesive or not for the cells), PAR or PLO, respectively, can be selected. This makes our nanocoating system a highly versatile tool for the prevention and therapy against multiple pathogens, specially ESKAPE pathogens. Moreover, pathogens presenting antibiotic resistance against classical drugs can be eradicated. *In vivo* investigations of the nanocoating system with an infected implant model, polymeric mesh used in hernia, demonstrated the strong potential of the strategy for future applications.

CRediT authorship contribution statement

Leyla Kocgozlu: Writing – original draft, Methodology, Formal analysis, Data curation, Conceptualization. **Angela Mutschler:** Writing – original draft, Methodology, Formal analysis, Data curation. **Lorène Tallet:** Formal analysis, Data curation, Conceptualization. **Cynthia Calligaro:** Formal analysis, Data curation, Conceptualization. **Helena Knopf-Marques:** Formal analysis, Data curation, Conceptualization. **Eloïse Lebaudy:** Formal analysis, Data curation, Conceptualization. **Eric Mathieu:** Investigation, Formal analysis, Conceptualization. **Morgane Rabineau:** Methodology, Formal analysis, Data curation. **Varvara Gribova:** Writing – review & editing, Methodology, Data curation, Conceptualization. **Bernard Senger:** Formal analysis, Data curation, Conceptualization. **N. Engin Vrana:** Writing – review & editing, Funding acquisition, Formal analysis, Data curation. **Philippe Lavalle:** Writing – review & editing, Funding acquisition, Formal analysis, Conceptualization.

Declaration of competing interest

The authors declare the following financial interests/personal relationships which may be considered as potential competing interests: Vrana reports financial support was provided by European Union. Lavalle reports financial support was provided by La Région Grand Est. If there are other authors, they declare that they have no known competing financial interests or personal relationships that could have appeared to influence the work reported in this paper.
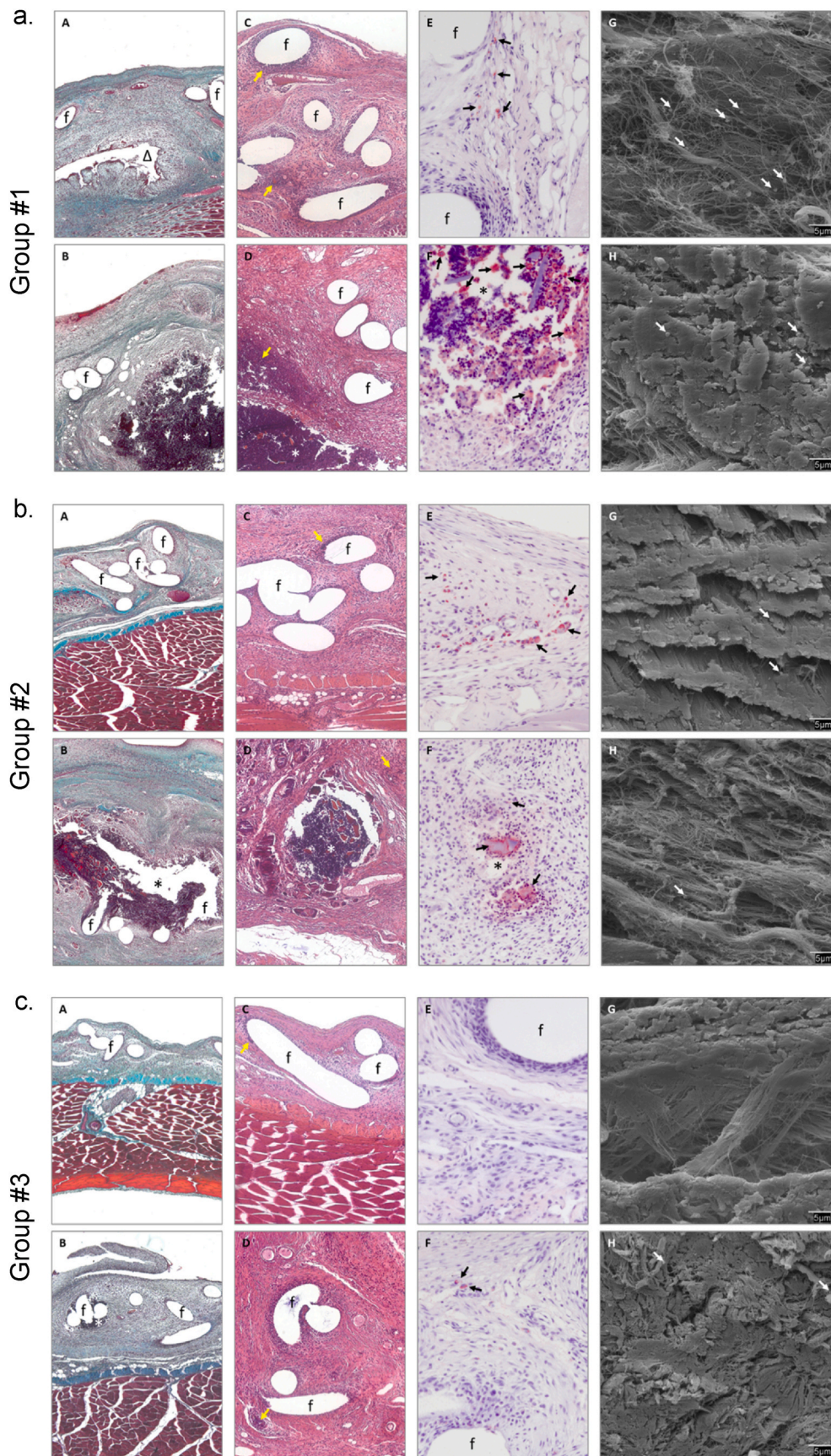
(caption on next page)

Fig. 10. Histological evaluation of the implants from group#1, 2 and 3 (a, b and c). (A, B) Neoformed connective tissue exhibiting accumulation of tissue exudate (Δ) and large abscesses (*) (Masson's trichrome, x50). (C, D) Detail of the inflammatory cells (yellow arrows) surrounding the mesh filaments (f) and the abscesses (hematoxylin eosin, x100). (E, F) Labeled bacteria (black arrows) were located either in the neoformed tissue and within the abscesses (*S. aureus* immunolabeling, x320). (G, H) Visualization by SEM at high magnification c (x 2000) to check the presence or of bacteria (white arrows) throughout the implant. (For interpretation of the references to colour in this figure legend, the reader is referred to the Web version of this article.)

Data availability

Data will be made available on request.

Acknowledgment

Appendix A. Supplementary data

Supplementary data to this article can be found online at https://doi.org/10.1016/j.mtbio.2024.101168.

Abbreviations

AFM	Atomic force microscope
ALG	Alginate
BSA	bovine serum albumin
C. albicans	*Candida albicans*
CHX	Chlorhexidine
CFU	Colony forming unit
CTC	5-cyano-2-3-ditolyl tetrazolium chloride
CSA	Chondroitin sulfate A
DMEM	Dulbecco's modified eagles medium
E. coli	*Escherichia coli*
EDC/NHS	N-Ethyl-N′-(3-(dimethylamino)propyl)carbodiimide hydrochloride/N-Hydroxysuccinimide
E. faecalis	*Enterococcus faecalis*
ELISA	enzyme-linked immunosorbent assay
FBS	Fetal bovine serum
FITC	Fluorescein isothiocyanate
FRAP	Fluorescence recovery after photobleaching
HA	Hyaluronic acid
HEP	Heparin
HEPES	4-(2-hydroxyethyl)-1-piperazineethanesulfonic acid
HUVEC	Human umbilical vein endothelial cell
IFN	interferon
IL	Interleukin
Im	intramuscular
LB	Lysogeny broth
LbL	Layer-by-layer
LM	Light microscopy
MDCK	Madin-Darby canine kidney
MRSA	Methicilin-resistant *S. aureus*
MHB	Mueller Hinton broth
MIC	Minimal inhibitory concentration
M. luteus	*Micrococcus luteus*
MTT	3-(4,5-dimethylthiazol-2-yl)-2,5-diphenyltetrazolium bromide
NO	Nitric oxide
NPD	neutralizing pharmacopoeia diluent
OD	optical density
P. aeruginosa	*Pseudomonas aeruginosa*
PAR	Poly(L-arginine)
PBS	Phosphate-buffered saline
PFA	Paraformaldehyde
PLL	Poly(L-lysine)
PLO	Poly(L-ornithine)
PGA	Poly(L-glutamic acid)
PSS	Poly(Sodium-4 styrene Sulfonate)
QCM-D	Quartz crystal microbalance with dissipation monitoring
S. aureus	*Staphylococcus aureus*
Sc	subcutaneous
S. epidermidis	*Staphylococcus epidermidis*
SEM	Scanning electron microscope
TBS	tris-buffered saline
TNF	tumor necrosis factor
Tris	tris (hydroxymethyl)-aminomethane
TRITC	tetramethylrhodamine
TSYEA	Tryptone Soya Yeast Extract Agar

References

[1] T. Pulingam, T. Parumasivam, A.M. Gazzali, A.M. Sulaiman, J.Y. Chee, M. Lakshmanan, C.F. Chin, K. Sudesh, Antimicrobial resistance: prevalence, economic burden, mechanisms of resistance and strategies to overcome, Eur. J. Pharmaceut. Sci. 170 (2022) 106103.

[2] R. Laxminarayan, The overlooked pandemic of antimicrobial resistance, Lancet 399 (10325) (2022) 606–607.

[3] C.M. Morel, R.A. Alm, C. Ardal, A. Bandera, G.M. Bruno, E. Carrara, G.L. Colombo, M.E.A. de Kraker, S. Essack, I. Frost, B. Gonzalez-Zorn, H. Goossens, L. Guardabassi, S. Harbarth, P.S. Jorgensen, S.S. Kanj, T. Kostyanev, R. Laxminarayan, F. Leonard, G.L. Hara, M. Mendelson, M. Mikulska, N.T. Mutters, K. Outterson, J.R. Bano, E. Tacconelli, L. Scudeller, G.A.-O. network, A one health framework to estimate the cost of antimicrobial resistance, Antimicrob. Resist. Infect. Control 9 (1) (2020) 187.

[4] K.G. Tarakji, C.R. Ellis, P. Defaye, C. Kennergren, Cardiac implantable electronic device infection in patients at risk, Arrhythmia Electrophysiol. Rev. 5 (1) (2016) 65–71.

[5] E. Klein, D.L. Smith, R. Laxminarayan, Hospitalizations and deaths caused by methicillin-resistant Staphylococcus aureus, United States, 1999-2005, Emerg. Infect. Dis. 13 (12) (2007) 1840–1846.

[6] S.Y. Tong, J.S. Davis, E. Eichenberger, T.L. Holland, V.G. Fowler Jr., Staphylococcus aureus infections: epidemiology, pathophysiology, clinical manifestations, and management, Clin. Microbiol. Rev. 28 (3) (2015) 603–661.

[7] V.G. Fowler Jr., J.M. Miro, B. Hoen, C.H. Cabell, E. Abrutyn, E. Rubinstein, G. R. Corey, D. Spelman, S.F. Bradley, B. Barsic, P.A. Pappas, K.J. Anstrom, D. Wray, C.Q. Fortes, I. Anguera, E. Athan, P. Jones, J.T. van der Meer, T.S. Elliott, D. P. Levine, A.S. Bayer, I.C.E. Investigators, Staphylococcus aureus endocarditis: a consequence of medical progress, JAMA 293 (24) (2005) 3012–3021.

[8] J. Zhang, M. Liu, H. Guo, S. Gao, Y. Hu, G. Zeng, D. Yang, Nanotechnology-driven strategies to enhance the treatment of drug-resistant bacterial infections, Wiley Interdiscip Rev Nanomed Nanobiotechnol 16 (3) (2024) e1968.

[9] C. Mas-Moruno, B. Su, M.J. Dalby, Multifunctional coatings and nanotopographies: toward cell instructive and antibacterial implants, Adv. Healthcare Mater. 8 (1) (2019) e1801103.

[10] L. Seon, P. Lavalle, P. Schaaf, F. Boulmedais, Polyelectrolyte multilayers: a versatile tool for preparing antimicrobial coatings, Langmuir 31 (47) (2015) 12856–12872.

[11] Y. Zou, Y.X. Zhang, Q. Yu, H. Chen, Dual-function antibacterial surfaces to resist and kill bacteria: painting a picture with two brushes simultaneously, J. Mater. Sci. Technol. 70 (2021) 24–38.

[12] Y. Zou, C.X. Liu, H.X. Zhang, Y. Wu, Y.C. Lin, J.J. Cheng, K.Y. Lu, L.H.Z. Li, Y. X. Zhang, H. Chen, Q. Yu, Three lines of defense: a multifunctional coating with anti-adhesion, bacteria-killing and anti-quorum sensing properties for preventing biofilm formation of Pseudomonas aeruginosa, Acta Biomater. 151 (2022) 254–263.

[13] G. Kay, E.L. Eby, B. Brown, J. Lyon, S. Eggington, G. Kumar, E. Fenwick, M. R. Sohail, D.J. Wright, Cost-effectiveness of TYRX absorbable antibacterial envelope for prevention of cardiovascular implantable electronic device infection, J. Med. Econ. 21 (3) (2018) 294–300.

[14] Y. Kondo, M. Ueda, Y. Kobayashi, J.O. Schwab, New horizon for infection prevention technology and implantable device, J Arrhythm 32 (4) (2016) 297–302.

[15] P. Lavalle, C. Picart, J. Mutterer, C. Gergely, H. Reiss, J.C. Voegel, B. Senger, P. Schaaf, Modeling the buildup of polyelectrolyte multilayer films having exponential growth, J. Phys. Chem. B 108 (2) (2004) 635–648.

[16] H. Ozcelik, N.E. Vrana, A. Gudima, V. Riabov, A. Gratchev, Y. Haikel, M.H. Metz-Boutigue, A. Carrado, J. Faerber, T. Roland, H. Kluter, J. Kzhyshkowska, P. Schaaf, P. Lavalle, Harnessing the multifunctionality in nature: a bioactive agent release system with self-antimicrobial and immunomodulatory properties, Adv. Healthcare Mater. 4 (13) (2015) 2026–2036.

[17] A. Mutschler, L. Tallet, M. Rabineau, C. Dollinger, M.H. Metz-Boutigue, F. Schneider, B. Senger, N.E. Vrana, P. Schaaf, P. Lavalle, Unexpected bactericidal activity of poly(arginine)/hyaluronan nanolayered coatings, Chem. Mater. 28 (23) (2016) 8700–8709.

[18] A. Mutschler, C. Betscha, V. Ball, B. Senger, N.E. Vrana, F. Boulmedais, A. Schroder, P. Schaaf, P. Lavalle, Nature of the polyanion governs the antimicrobial properties of poly(arginine)/polyanion multilayer films, Chem. Mater. 29 (7) (2017) 3195–3201.

[19] K. Colville, N. Tompkins, A.D. Rutenberg, M.H. Jericho, Effects of poly(L-lysine) substrates on attached Escherichia coli bacteria, Langmuir 26 (4) (2010) 2639–2644.

[20] T. Yoshida, T. Nagasawa, epsilon-Poly-L-lysine: microbial production, biodegradation and application potential, Appl. Microbiol. Biotechnol. 62 (1) (2003) 21–26.

[21] C.P. Johnson, H.Y. Tang, C. Carag, D.W. Speicher, D.E. Discher, Forced unfolding of proteins within cells, Science 317 (5838) (2007) 663–666.

[22] M. Pan, C. Lu, M. Zheng, W. Zhou, F. Song, W. Chen, F. Yao, D. Liu, J. Cai, Unnatural amino-acid-based star-shaped poly(l-ornithine)s as emerging long-term and biofilm-disrupting antimicrobial peptides to treat Pseudomonas aeruginosa-infected burn wounds, Adv. Healthcare Mater. 9 (19) (2020) e2000647.

[23] A.C. Quiroga-Centeno, C.A. Quiroga-Centeno, S. Guerrero-Macias, O. Navas-Quintero, S.A. Gomez-Ochoa, Systematic review and meta-analysis of risk factors for mesh infection following abdominal wall hernia repair surgery, Am. J. Surg. 224 (1 Pt A) (2022) 239–246.

[24] B. Perez-Kohler, Y. Bayon, J.M. Bellon, Mesh infection and hernia repair: a review, Surg. Infect. 17 (2) (2016) 124–137.

[25] O. Guillaume, R. Perez-Tanoira, R. Fortelny, H. Redl, T.F. Moriarty, R.G. Richards, D. Eglin, A. Petter Puchner, Infections associated with mesh repairs of abdominal wall hernias: are antimicrobial biomaterials the longed-for solution? Biomaterials 167 (2018) 15–31.

[26] F. Gossetti, L. D'Amore, E. Annesi, P. Bruzzone, L. Bambi, M.R. Grimaldi, F. Ceci, P. Negro, Mesh-related visceral complications following inguinal hernia repair: an emerging topic, Hernia 23 (4) (2019) 699–708.

[27] D.M.P. De Oliveira, B.M. Forde, T.J. Kidd, P.N.A. Harris, M.A. Schembri, S. A. Beatson, D.L. Paterson, M.J. Walker, Antimicrobial resistance in ESKAPE pathogens, Clin. Microbiol. Rev. 33 (3) (2020).

[28] M.S. Mulani, E.E. Kamble, S.N. Kumkar, M.S. Tawre, K.R. Pardesi, Emerging strategies to combat ESKAPE pathogens in the era of antimicrobial resistance: a review, Front. Microbiol. 10 (2019) 539.

[29] M.V. Voinova, M. Rodahl, M. Jonson, B. Kasemo, Viscoelastic acoustic response of layered polymer films at fluid-solid interfaces: continuum mechanics approach, Phys. Scripta 59 (5) (1999) 391–396.

[30] M. Fernandez-Gutierrez, E. Olivares, G. Pascual, J.M. Bellon, J. San Roman, Low-density polypropylene meshes coated with resorbable and biocompatible hydrophilic polymers as controlled release agents of antibiotics, Acta Biomater. 9 (4) (2013) 6006–6018.

[31] B. Perez-Kohler, F. Garcia-Moreno, T. Brune, G. Pascual, J.M. Bellon, Preclinical bioassay of a polypropylene mesh for hernia repair pretreated with antibacterial solutions of chlorhexidine and allicin: an in vivo study, PLoS One 10 (11) (2015) e0142768.

[32] B. Perez-Kohler, S. Benito-Martinez, M. Rodriguez, F. Garcia-Moreno, G. Pascual, J. M. Bellon, Experimental study on the use of a chlorhexidine-loaded carboxymethylcellulose gel as antibacterial coating for hernia repair meshes, Hernia 23 (4) (2019) 789–800.

[33] P. Lavalle, J.C. Voegel, D. Vautier, B. Senger, P. Schaaf, V. Ball, Dynamic aspects of films prepared by a sequential deposition of species: perspectives for smart and responsive materials, Adv. Mater. 23 (10) (2011) 1191–1221.

[34] L. Jourdainne, S. Lecuyer, Y. Arntz, C. Picart, P. Schaaf, B. Senger, J.C. Voegel, P. Lavalle, T. Charitat, Dynamics of poly(L-lysine) in hyaluronic acid/poly(L-lysine) multilayer films studied by fluorescence recovery after pattern photobleaching, Langmuir 24 (15) (2008) 7842–7847.

[35] C. Porcel, P. Lavalle, G. Decher, B. Senger, J.C. Voegel, P. Schaaf, Influence of the polyelectrolyte molecular weight on exponentially growing multilayer films in the linear regime, Langmuir 23 (4) (2007) 1898–1904.

[36] A. Tezcaner, D. Hicks, F. Boulmedais, J. Sahel, P. Schaaf, J.C. Voegel, P. Lavalle, Polyelectrolyte multilayer films as substrates for photoreceptor cells, Biomacromolecules 7 (1) (2006) 86–94.

[37] M.F. Sampedro, R. Patel, Infections associated with long-term prosthetic devices, Infect. Dis. Clin. 21 (3) (2007) 785–819, x.

[38] C. von Eiff, B. Jansen, W. Kohnen, K. Becker, Infections associated with medical devices: pathogenesis, management and prophylaxis, Drugs 65 (2) (2005) 179–214.

[39] L. Kocgozlu, P. Lavalle, G. Koenig, B. Senger, Y. Haikel, P. Schaaf, J.C. Voegel, H. Tenenbaum, D. Vautier, Selective and uncoupled role of substrate elasticity in the regulation of replication and transcription in epithelial cells, J. Cell Sci. 123 (Pt 1) (2010) 29–39.

[40] A. Schneider, G. Francius, R. Obeid, P. Schwinte, J. Hemmerle, B. Frisch, P. Schaaf, J.C. Voegel, B. Senger, C. Picart, Polyelectrolyte multilayers with a tunable Young's modulus: influence of film stiffness on cell adhesion, Langmuir 22 (3) (2006) 1193–1200.

[41] G. Blin, N. Lablack, M. Louis-Tisserand, C. Nicolas, C. Picart, M. Puceat, Nano-scale control of cellular environment to drive embryonic stem cells selfrenewal and fate, Biomaterials 31 (7) (2010) 1742–1750.

[42] H. Chang, X.Q. Liu, M. Hu, H. Zhang, B.C. Li, K.F. Ren, T. Boudou, C. Albiges-Rizo, C. Picart, J. Ji, Substrate stiffness combined with hepatocyte growth factor modulates endothelial cell behavior, Biomacromolecules 17 (9) (2016) 2767–2776.

[43] L. Kocgozlu, T.B. Saw, A.P. Le, I. Yow, M. Shagirov, E. Wong, R.M. Mege, C.T. Lim, Y. Toyama, B. Ladoux, Epithelial cell packing induces distinct modes of cell extrusions, Curr. Biol. 26 (21) (2016) 2942–2950.

[44] G.T. Eisenhoffer, P.D. Loftus, M. Yoshigi, H. Otsuna, C.-B. Chien, P.A. Morcos, J. Rosenblatt, Crowding induces live cell extrusion to maintain homeostatic cell numbers in epithelia, Nature 484 (7395) (2012) 546.

[45] W.J. Liu, G.L. Zhang, J.R. Wu, Y.L. Zhang, J. Liu, H.Y. Luo, L.Q. Shao, Insights into the angiogenic effects of nanomaterials: mechanisms involved and potential applications, J. Nanobiotechnol. 18 (1) (2020) 22.

[46] T. Li, T. Zhang, The application of nanomaterials in angiogenesis, Curr. Stem Cell Res. Ther. 16 (1) (2021) 74–82.

[47] L. Yang, L.H. Li, L. Jiang, J.Q. Pan, R.F. Luo, Y.B. Wang, Micelle-embedded coating with ebselen for nitric oxide generation, Med. Gas Res. 9 (4) (2019) 176–183.

[48] J. Loscalzo, G. Welch, Nitric oxide and its role in the cardiovascular system, Prog. Cardiovasc. Dis. 38 (2) (1995) 87–104.

[49] J.C. Stoclet, E. Troncy, B. Muller, C. Brua, A.L. Kleschyov, Molecular mechanisms underlying the role of nitric oxide in the cardiovascular system, Expet Opin. Invest. Drugs 7 (11) (1998) 1769–1779.

[50] D. Tousoulis, A.M. Kampoli, C. Tentolouris, N. Papageorgiou, C. Stefanadis, The role of nitric oxide on endothelial function, Curr. Vasc. Pharmacol. 10 (1) (2012) 4–18.

[51] J.D. Luo, A.F. Chen, Nitric oxide: a newly discovered function on wound healing, Acta Pharmacol. Sin. 26 (3) (2005) 259–264.

[52] H. Schmidt, H. Nau, W. Wittfoht, J. Gerlach, K.E. Prescher, M.M. Klein, F. Niroomand, E. Bohme, Arginine is a physiological precursor of endothelium-derived nitric-oxide, Eur. J. Pharmacol. 154 (2) (1988) 213–216.

[53] R.M.J. Palmer, D.D. Rees, D.S. Ashton, S. Moncada, L-arginine is the physiological precursor for the formation of nitric-oxide in endothelium-dependent relaxation, Biochem Bioph Res Co 153 (3) (1988) 1251–1256.

[54] L. Castillo, M. Sanchez, J. Vogt, T.E. Chapman, T.C. DeRojas-Walker, S. R. Tannenbaum, A.M. Ajami, V.R. Young, Plasma arginine, citrulline, and ornithine kinetics in adults, with observations on nitric oxide synthesis, Am. J. Physiol. 268 (2 Pt 1) (1995) E360–E367.

[55] D.J. Mitchell, D.T. Kim, L. Steinman, C.G. Fathman, J.B. Rothbard, Polyarginine enters cells more efficiently than other polycationic homopolymers, J. Pept. Res. 56 (5) (2000) 318–325.

[56] T. Kvasnicka, [NO (nitric oxide) and its significance in regulation of vascular homeostasis], Vnitr. Lek. 49 (4) (2003) 291–296.

[57] M.W. Radomski, S. Moncada, Regulation of vascular homeostasis by nitric oxide, Thromb. Haemostasis 70 (1) (1993) 36–41.

[58] A. European Food Safety, P. European Centre for Disease, Control, the European Union Summary Report on Antimicrobial Resistance in zoonotic and indicator bacteria from humans, animals and food in 2018/2019, EFSA J. 19 (4) (2021) e06490.

[59] P.M. Nischal, First global report on antimicrobial resistance released by the WHO, Natl. Med. J. India 27 (4) (2014) 241.

[60] A.P. Pallett, E.G. Smyth, Clinicians' guide to antibiotics. Tetracycline, Br. J. Hosp. Med. 40 (5) (1988) 385–390.

[61] N. Stoikes, G.R. Voeller, New developments in hernia repair: a 2013 update, Surg. Technol. Int. 23 (2013) 107–111.

[62] K. Ronka, J. Vironen, J. Kossi, S. Hulmi, T. Silvasti, T. Hakala, I. Ilves, I. Song, M. Hertsi, P. Juvonen, H. Paajanen, Randomized multicenter trial comparing glue fixation, self-gripping mesh, and suture fixation of mesh in lichtenstein hernia repair (FinnMesh study), Ann. Surg. 262 (5) (2015) 714–719. ; discussion 719-20.

[63] T.M. Karpinski, A.K. Szkaradkiewicz, Chlorhexidine-pharmaco-biological activity and application, Eur. Rev. Med. Pharmacol. Sci. 19 (7) (2015) 1321–1326.